Inorganic Chemistry

Article

Iridium Ziegler-Type Hydrogenation Catalysts Made from [(1,5-COD)Ir(μ-O$_2$C$_8$H$_{15}$)]$_2$ and AlEt$_3$: Spectroscopic and Kinetic Evidence for the Ir$_n$ Species Present and for Nanoparticles as the Fastest Catalyst

William M. Alley,[†] Isil K. Hamdemir,[†] Qi Wang,[‡] Anatoly I. Frenkel,[‡] Long Li,[§] Judith C. Yang,[§] Laurent D. Menard,[∥] Ralph G. Nuzzo,[∥] Saim Özkar,[⊥] Kimberly A. Johnson,[#] and Richard G. Finke*,[†]

[†]*Department of Chemistry, Colorado State University, Fort Collins, Colorado 80523,* [‡]*Department of Physics, Yeshiva University, New York, New York 10016,* [§]*University of Pittsburgh, Pittsburgh, Pennsylvania 15261,* [∥]*University of Illinois, Urbana, Illinois 61801,* [⊥]*Department of Chemistry, Middle East Technical University, 06531 Ankara, Turkey, and* [#]*Shell Oil Company, Houston, Texas 77082*

Ziegler-type hydrogenation catalysts, those made from a group 8−10 transition metal precatalyst and an AlR$_3$ cocatalyst, are often used for large scale industrial polymer hydrogenation; note that Ziegler-type *hydrogenation* catalysts are *not* the same as Ziegler−Natta *polymerization* catalysts. A review of prior studies of Ziegler-type hydrogenation catalysts (Alley et al. *J. Mol. Catal. A: Chem.* **2010,** *315,* 1−27) reveals that a ∼50 year old problem is identifying the metal species present before, during, and after Ziegler-type hydrogenation catalysis, and which species are the kinetically best, fastest catalysts—that is, which species are the true hydrogenation catalysts. Also of significant interest is whether what we have termed "Ziegler nanoclusters" are present and what their relative catalytic activity is. Reported herein is the characterization of an Ir Ziegler-type hydrogenation catalyst, a valuable model (*vide infra*) for the Co-based industrial Ziegler-type hydrogenation catalyst, made from the crystallographically characterized [(1,5-COD)Ir(μ-O$_2$C$_8$H$_{15}$)]$_2$ precatalyst plus AlEt$_3$. Characterization of this Ir model system is accomplished before and after catalysis using a battery of physical methods including Z-contrast scanning transmission electron microscopy (STEM), high resolution (HR)TEM, and X-ray absorption fine structure (XAFS) spectroscopy. Kinetic studies plus Hg(0) poisoning experiments are then employed to probe which species are the fastest catalysts. The main findings herein are that (i) a combination of the catalyst precursors [(1,5-COD)Ir(μ-O$_2$C$_8$H$_{15}$)]$_2$ and AlEt$_3$ gives catalytically active solutions containing a broad distribution of Ir$_n$ species ranging from monometallic Ir complexes to nanometer scale, noncrystalline Ir$_n$ nanoclusters (up to Ir$_{\sim100}$ by Z-contrast STEM) with the estimated mean Ir species being 0.5−0.7 nm, Ir$_{\sim4−15}$ clusters considering the similar, but not identical results from the different analytical methods; furthermore, (ii) the mean Ir$_n$ species are practically the same regardless of the Al/Ir ratio employed, suggesting that the observed changes in catalytic activity at different Al/Ir ratios are primarily the result of changes in the form or function of the Al-derived component (and not due to significant AlEt$_3$-induced changes in initial Ir$_n$ nuclearity). However (iii), during hydrogenation, a shift in the population of Ir species toward roughly 1.0−1.6 nm, *fcc* Ir(0)$_{\sim40−150}$, Ziegler nanoclusters occurs with, significantly, (iv) *a concomitant increase in catalytic activity.* Importantly, and although catalysis by discrete subnanometer Ir species is not ruled out by this study, (v) the increases in activity with increased nanocluster size, plus Hg(0) poisoning studies, provide the best evidence to date that the approximately 1.0−1.6 nm, *fcc* Ir(0)$_{\sim40−150}$, heterogeneous Ziegler nanoclusters are the fastest catalysts in this industrially related catalytic hydrogenation system (and in the simplest, Ockham's Razor interpretation of the data). In addition, (vi) Ziegler nanoclusters are confirmed to be an unusual, hydrocarbon-soluble, highly coordinatively unsaturated, Lewis-acid containing, and highly catalytically active type of nanocluster for use in other catalytic applications and other areas.

Introduction

Ziegler-type hydrogenation catalysts prepared, by definition, from a nonzero valent group 8−10 transition metal precatalyst combined with an AlR$_3$ cocatalyst, such as triethylaluminum (AlEt$_3$), account for much of the worldwide industrial hydrogenation of styrenic block copolymers (SBCs).[1] According to one estimate, hydrogenated SBCs are produced at a rate in excess of 1.7×10^5 metric tons annually worldwide.[2] The literature concerning Ziegler-type hydrogenation catalysts has

*To whom correspondence should be addressed. E-mail: rfinke@lamar.colostate.edu.

(1) Johnson, K. A. *Polym. Prepr.* **2000,** *41,* 1525–1526.
(2) Alley, W. M.; Girard, C. W.; Özkar, S.; Finke, R. G. *Inorg. Chem.* **2009,** *48,* 1114–1121.

recently been critically reviewed by us,[3] leading to the following insights: (i) Improved fundamental understanding of Ziegler-type hydrogenation catalysts is needed so that rationally directed catalyst improvements can be made. (ii) Multiple variables are important in catalyst synthesis, including the specific components used, the cocatalyst/transition metal ratio (Al/M), the amount of H_2O present (widely observed to be connected to the amount of cocatalyst), and the order of addition of the catalyst components, and (iii) these variables influence the nature of the resulting catalysts and their catalytic properties. Other insights[3] are (iv) a central, unanswered question in the area of Ziegler-type industrial hydrogenation catalysts is whether the true catalyst is a homogeneous (e.g., single metal organometallic) or heterogeneous (e.g., polymetallic $M(0)_n$ nanocluster) catalyst,[4] and that (v) the most recent, especially noteworthy prior work—that of Shmidt and co-workers,[5] and Bönnemann and co-workers[3,6]—is starting to *suggest* that Ziegler-type hydrogenation catalysts are transition metal nanoclusters, what we have coined in our review as "Ziegler nanoclusters".[3] However, (vi) compelling or even highly suggestive evidence concerning the homogeneous versus heterogeneous catalysis question for Ziegler-type hydrogenation catalysts has remained elusive due to the use of often poorly defined precursors or the lack of application of the best current, previously successful approaches for addressing the historically perplexing "is it homogeneous or heterogeneous catalysis?" question.[7] *Absent in particular are definitive kinetic studies connected to knowledge of the dominant form(s) of the transition metal catalyst.* On the basis of our review of the literature, we reasoned, therefore, that (vii) the use of a well-characterized precatalyst as a model for the industrially favored, but often less well- (or clearly) characterized, Co and Ni precatalysts might allow new insights into Ziegler-type hydrogenation catalyst systems, and (viii) that our previously successful, multipronged, kinetic-containing approach for addressing the homogeneous versus heterogeneous catalysis problem[3,4b,7,8] should be applied to Ziegler-type,

industrially relevant hydrogenation catalysts. In addition, (ix) we reasoned that the use of the third row transition metal Ir, where strong Ir–Ir bonds, and for example $Ir(0)_n$ nanoclusters that are typically stable under characterization conditions,[7a] might prove very useful—if not necessary—in allowing identification of the dominant species present before and after catalysis without significant artifacts due to the use of ex situ or even in situ (as opposed to the ideal operando[9]) methods.

Herein, we report the characterization of iridium model Ziegler-type hydrogenation catalysts made from the crystallographically characterized precatalyst, $[(1,5\text{-}COD)Ir(\mu\text{-}O_2\text{-}C_8H_{15})]_2$,[2] plus $AlEt_3$ under carefully controlled conditions. The resultant pre- and posthydrogenation catalyst materials are characterized by a variety of analytical techniques including Z-contrast scanning transmission electron microscopy (STEM), high resolution (HR)TEM, X-ray absorption fine structure (XAFS) spectroscopy, and matrix assisted laser desorption ionization mass spectrometry (MALDI MS).[10] The needed kinetic and Hg(0) poisoning studies round out the work reported herein. The main findings are (i) that combining the catalyst precursors $[(1,5\text{-}COD)Ir(\mu\text{-}O_2C_8H_{15})]_2$ and $AlEt_3$ gives catalytically active solutions containing Ir_n clusters with a range of sizes from monometallic Ir complexes to nanometer scale, noncrystalline Ir_n nanoclusters with an estimated mean 0.5−0.7 nm, $Ir_{\sim4-15}$ cluster (considering the similar, but not identical results obtained from the different analytical methods), *but* (ii) that during the hydrogenation process, the development of roughly 1.0−1.6 nm, *fcc* $Ir(0)_{\sim40-150}$ nanoclusters occurs, and (iii) that kinetic studies indicate, a concomitant *increase in catalytic activity* as the size of the Ir_n nanoclusters increases. In addition, we find (iv) that this size−activity correlation, plus Hg(0) poisoning studies, suggest (as the simplest, "Ockham's razor" interpretation of the data) that the fastest, kinetically competent catalysts are the larger, roughly 1.0−1.6 nm, $Ir(0)_{\sim40-150}$ nanoclusters rather than the monometallic complexes and 0.5−0.7 nm, $Ir_{\sim4-15}$ clusters initially present (the homogeneous catalyst component alone appears to have about 5% of the activity of the overall catalyst solution, vide infra).

The results are significant in comparison to even the ~50 year history of Ziegler-type hydrogenation catalysts[3] (a) in being the first to show that the transition metal component of the initial catalyst formation reaction is, at least for the present Ir model system, a broadly disperse mixture ranging from mono-Ir complexes to noncrystalline nanoscale clusters, with the estimated mean Ir_n species being 0.5−0.7 nm, $Ir_{\sim4-15}$ clusters; (b) in being the first report of the explicit application of an established, previously successful, multiprong approach for addressing the homogeneous versus heterogeneous catalysis problem in a Ziegler-type hydrogenation catalyst system;[3,4b,7,8] and (c) in providing evidence consistent with and highly supportive of the now dominant hypothesis for future research

(3) Alley, W. M.; Hamdemir, I. K.; Johnson, K. A.; Finke, R. G. *J. Mol. Catal. A: Chem.* **2010**, *315*, 1–27.

(4) (a) Collman, J. P.; Hegedus, L. S.; Norton, J. R.; Finke, R. G. *Principles and Applications of Organotransition Metal Chemistry*; University Science Books: Mill Valley, CA, 1987. (b) Widegren, J.; Finke, R. *J. Mol. Catal. A: Chem.* **2003**, *198*, 317–341. (c) Schwartz, J. *Acc. Chem. Res.* **1985**, *18*, 302–308.

(5) (a) Shmidt, F. K.; Nindakova, L. O.; Shainyan, B. A.; Saraev, V. V.; Chipanina, N. N.; Umanetz, V. A. *J. Mol. Catal. A: Chem.* **2005**, *235*, 161–172. (b) Belykh, L. B.; Titova, Yu. Yu.; Umanets, V. A.; Shmidt, F. K. *Russ. J. Appl. Chem.* **2006**, *79*, 1271–1277. (c) Nindakova, L. O.; Shmidt, F. K.; Saraev, V. V.; Shainyan, B. A.; Chipanina, N. N.; Umanets, V. A.; Belonogova, L. N.; Toryashinova, D.-S. D. *Kinet. Catal.* **2006**, *47*, 54–63. (d) Belykh, L. B.; Goremyka, T. V.; Skripov, N. I.; Umanets, V. A.; Shmidt, F. K. *Kinet. Catal.* **2006**, *47*, 367–374.

(6) (a) Bönnemann, H.; Brijoux, W.; Brinkmann, R.; Endruschat, U.; Hofstadt, W.; Angermund, K. *Rev. Roum. Chim.* **1999**, *44*, 1003–1010. (b) Bönnemann, H.; Waldöfner, N.; Haubold, H.-G.; Vad, T. *Chem. Mater.* **2002**, *14*, 1115–1120. (c) Angermund, K.; Bühl, M.; Dinjus, E.; Endruschat, U.; Gassner, F.; Haubold, H.-G.; Hormes, J.; Köhl, G.; Mauschick, F. T.; Modrow, H.; Mörtel, R.; Mynott, R.; Tesche, B.; Vad, T.; Waldöfner, N.; Bönnemann, H. *Angew. Chem., Int. Ed.* **2002**, *41*, 4041–4044. (d) Angermund, K.; et al. *J. Phys. Chem. B* **2003**, *107*, 7507–7515. (e) Haubold, H.-G.; Vad, T.; Waldöfner, N.; Bönnemann, H. *J. Appl. Crystallogr.* **2003**, *36*, 617–620. (f) Wen, F.; Bönnemann, H.; Mynott, R. J.; Spliethoff, B.; Weidenthaler, C.; Palina, N.; Zinoveva, S.; Modrow, H. *Appl. Organomet. Chem.* **2005**, *19*, 827–829.

(7) (a) Lin, Y.; Finke, R. G. *Inorg. Chem.* **1994**, *33*, 4891–4910. (b) Aiken, J. D., III; Lin, Y.; Finke, R. G. *J. Mol. Catal. A: Chem.* **1996**, *114*, 29–51. (c) Widegren, J. A.; Bennett, M. A.; Finke, R. G. *J. Am. Chem. Soc.* **2003**, *125*, 10301–10310. (d) Hagen, C. M.; Widegren, J. A.; Maitlis, P. M.; Finke, R. G. *J. Am. Chem. Soc.* **2005**, *127*, 4423–4432. (e) Finney, E. E.; Finke, R. G. *Inorg. Chim. Acta* **2006**, *359*, 2879–2887.

(8) (a) Jaska, C. A.; Manners, I. *J. Am. Chem. Soc.* **2004**, *126*, 1334–1335. (b) Jaska, C. A.; Manners, I. *J. Am. Chem. Soc.* **2004**, *126*, 9776–9785. (c) Zahmakiran, M.; Özkar, S. *Inorg. Chem.* **2009**, *48*, 8955–8964.

(9) For lead references to operando studies of catalysis and their importance, see: (a) Thomas, J. M.; Somorjai, G. A. *Top. Catal.* **1999**, *8* (preface). (b) Weckhuysen, B. M. *Chem. Commun.* **2002**, 97–110. (c) Guerrero-Pérez, M. O.; Bañares, M. A. *Chem. Commun.* **2002**, 1292–1293. (d) Meunier, F.; Daturi, M. *Catal. Today* **2006**, *113*, 1–2.

(10) We were made aware of XAFS as a potentially highly valuable analytical technique for the study of Ziegler-type hydrogenation catalyst systems by the following excellent early studies: (a) Goulon, J.; Georges, E.; Goulon-Ginet, C.; Chauvin, Y.; Commereuc, D.; Dexpert, H.; Freund, E. *Chem. Phys.* **1984**, *83*, 357–366. (b) Esselin, C.; Bauer-Grosse, E.; Goulon, J.; Williams, C.; Chauvin, Y.; Commereuc, D.; Freund, E. *J. Phys. Colloques* **1986**, *47*, C8−243–C8−248.

Scheme 1. Catalyst Preparation and Hydrogenation of Cyclohexene Plus (shown to the right) the Single-Crystal X-Ray Diffraction Determined Structure of the [(1,5-COD)Ir(μ-O$_2$C$_8$H$_{15}$)]$_2$ Precatalyst (adapted with permission from ref 2, copyright 2009, American Chemical Society)
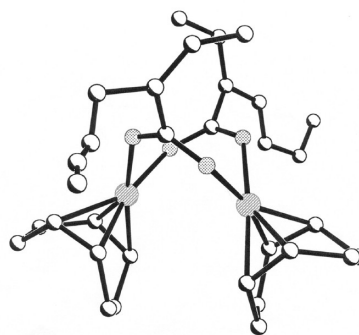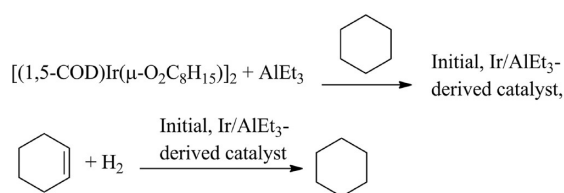
in the area, namely, that Ziegler nanoclusters appear to be the kinetically dominant catalysts—although we note that the true catalyst in the industrially fastest Co/AlR$_3$ system remains to be identified and is under investigation. As such, the findings reported herein are both believed to be important fundamentally and are expected to result in practical implications due to the large-scale industrial utilization of Ziegler-type hydrogenation catalysts.[11−14]

Results and Discussion

A key insight from our review of the literature of Ziegler-type hydrogenation catalysts[3] is that their catalytic hydrogenation activity is quite sensitive to a number of variables, including the specific conditions and details under which the catalysts are synthesized. Therefore, preliminary catalytic studies were carried out in order to determine appropriate, representative conditions for reliable and reproducible catalyst preparation and subsequent catalytic use as well as to ensure the broadest applicability of the results of the studies which follow.

Catalyst Preparation. Catalyst samples used in olefin hydrogenation were prepared by a combination of [(1,5-COD)Ir(μ-O$_2$C$_8$H$_{15}$)]$_2$ and AlEt$_3$, with Al/Ir ratios of 1.0, 2.0, 3.0, and 5.0. We previously reported the control experiment of using [(1,5-COD)Ir(μ-O$_2$C$_8$H$_{15}$)]$_2$ for catalytic cyclohexene hydrogenation *without* AlEt$_3$.[2] The resulting black, Ir(0) precipitate formed during hydrogenation indicates that the AlEt$_3$ component is crucial for the stability of the catalyst (and nanoclusters, vide infra). A brief summary of those hydrogenation results without AlEt$_3$ is provided in the Supporting Information for the interested reader.

In light of what is known from the literature,[3] all catalyst solutions were prepared using the same materials from the same sources. Also, the procedures described

below and in the Experimental Section were followed exactly for repeat kinetic runs. Specifically, an 18.0 mM cyclohexane solution of AlEt$_3$ was rapidly added to a cyclohexane solution of the precatalyst, 9.0 mM in [Ir], without the presence of the olefinic substrate, which has been reported to influence these specific catalyst formation reactions in some cases.[3] The addition of AlEt$_3$ to the cyclohexane solution of [(1,5-COD)Ir(μ-O$_2$C$_8$H$_{15}$)]$_2$ resulted in an immediate change in color from orange to tawny yellow, regardless of whether an Al/Ir ratio of 1.0, 2.0, 3.0, or 5.0 was used. Catalyst solutions were then used for the catalytic hydrogenation of the model olefin, cyclohexene, as depicted in Scheme 1.

Cyclohexene Hydrogenation Curves and Catalyst Aging. Example cyclohexene hydrogenation curves obtained by following H$_2$ pressure loss, and using the [(1,5-COD)Ir(μ-O$_2$C$_8$H$_{15}$)]$_2$ plus AlEt$_3$ catalysts with Al/Ir ratios of 1.0, 2.0, and 3.0, are shown in Figure 1. In each case, the Ir/AlEt$_3$-based catalysts exhibit immediate activity, but the maximum rate is attained later as the reaction proceeds, Figure 1a and b—that is, either more of the catalyst or a better catalyst is being formed as the reaction proceeds.

A key factor in the preparation of the catalyst is the time elapsed between mixing the [(1,5-COD)Ir(μ-O$_2$C$_8$H$_{15}$)]$_2$ and AlEt$_3$ components prior to use of the resultant solution for the test reaction of cyclohexene hydrogenation, hereafter referred to as the *aging time*. Despite the initial reaction between the Ir precatalyst and AlEt$_3$, hydrogenation activity approaches a maximum value if the initially prepared catalyst solutions are allowed to age by stirring under an atmosphere of N$_2$ for about 8−24 h before being placed under H$_2$ (Figure S2, Supporting Information); maximum rates of aged catalysts are ∼2−7-fold greater than the maximum rates of their nonaged counterparts, depending on Al/Ir. Without aging catalyst solutions before their use, the resulting hydrogenation curves exhibit a more distinct transition from a less active—but longer-persisting—initial stage to their maximum rate stage, especially at the Al/Ir ratio of 5.0 (Figure S3, Supporting Information). However, even 33 h of aging does not completely eliminate the slower initial rate (Figure S2b of the Supporting Information). The maximum rates are ∼2−10 times the initial rates in each case, depending on Al/Ir and whether or not catalyst solutions were aged. A table giving the mean initial and maximum rates from multiple runs of both aged and nonaged catalysts samples, and at various Al/Ir ratios, is given in the Supporting Information. Clearly, evolution of the catalyst is occurring,

(11) Further analysis of this catalyst system using additional kinetic studies reveals an *increase* in catalyst turnover frequency with *decreasing* [Ir] concentration and will be reported elsewhere.[12] Another important remaining question, one beyond the scope of this work, is what happens to the AlEt$_3$ cocatalyst; that is, what are the forms and roles of the AlR$_3$-derived component in the catalysis? That work is also currently underway and will be addressed in a separate paper.[13] Also addressed elsewhere is the question of the true active catalyst species in industrial Co and Ni Ziegler-type hydrogenation catalyst systems.[14]

(12) Alley, W. M.; Li, L.; Yang, J. C.; Özkar, S.; Finke, R. G. Manuscript in preparation.

(13) Hamdemir, I. K.; Özkar, S.; Johnson, K. A.; Finke, R. G. Manuscript in preparation.

(14) Alley, W. M.; Hamdemir, I. K.; Li, L.; Yang, J. C.; Wang, Q.; Frenkel, A.; Menard, L. D.; Nuzzo, R. G.; Özkar, S.; Johnson, K. A.; Finke, R. G. Manuscript in preparation.
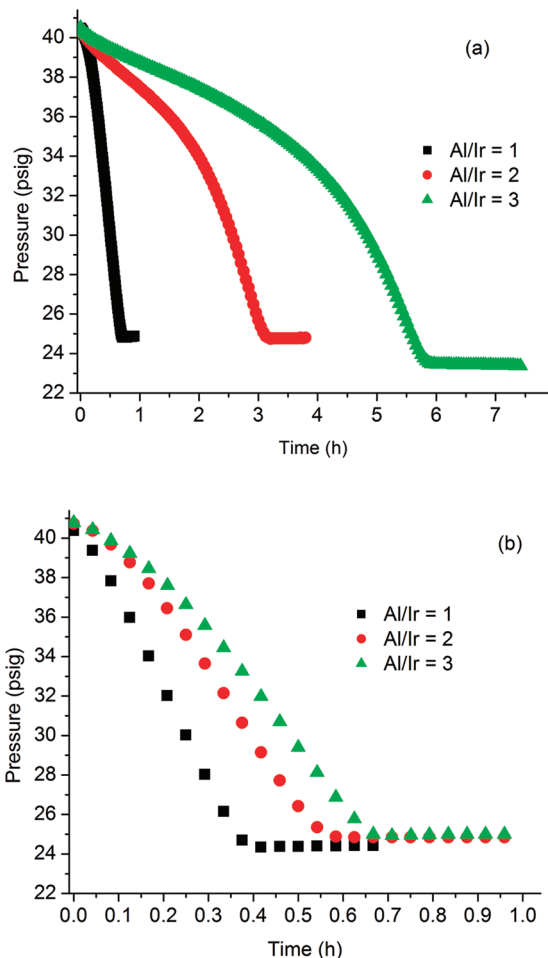
Figure 1. Catalytic cyclohexene hydrogenations using [(1,5-COD)Ir-(μ-O$_2$C$_8$H$_{15}$)]$_2$ plus AlEt$_3$ catalysts that were (a) used immediately after preparation or (b) first aged for 9 h with stirring under a N$_2$ atmosphere. Note the ca. 10-fold reduced time scale axis in part b versus that in part a—that is, the aged catalyst is about 2- to 7-fold more active, depending on the Al/Ir ratio, on the basis of the *maximum* hydrogenation rate achieved. In each case, the reaction is fastest just before the end of the catalytic run, despite the normal, rate-slowing decrease in olefin concentration and H$_2$ pressure (the max rate is $\sim$2−10 times the initial rate of a given run). Also, the effect on the initial rate of the Al/Ir ratio is significantly less when the catalyst solutions are aged before use. Reactions were performed in cyclohexane solutions, 0.6 mM in [Ir], initially 1.65 M in cyclohexene, at 22.0 °C, and stirred at 1000 ± 10 rpm. Additional catalytic hydrogenation curves, attained using catalysts with an Al/Ir ratio of 5.0, are shown in Figure S3 of the Supporting Information.

so that it became important to determine the nature of that evolution, vide infra.

As expected from the literature,[3] catalyst activity is dependent on the Al/Ir ratio. However, the magnitude of the effect of the Al/Ir ratio on the catalyst activity is diminished when the catalysts are aged. Interestingly, even 33 h of aging of the catalyst solutions does not result in further color change; yet, in all cases, the reaction solutions change color *during hydrogenation* (i.e., under H$_2$ and cyclohexene) to darker brown, results that are consistent with further catalyst development to larger Ir(0)$_n$ nanoclusters that have been identified by several physical methods, vide infra. Catalyst solutions sometimes give a dark brown/black precipitate within a few days of hydrogenation if the catalyst solution is transferred to a N$_2$ atmosphere shortly after complete consumption of the substrate. However, a dark brown/black

precipitate (Ir(0) by XPS) plus a clear, nearly colorless solution always results if the solutions are left under pressurized H$_2$ for extended amounts of time after complete consumption of the cyclohexene substrate. The observations of brown-black catalyst solutions plus metal(0) precipitates are strongly suggestive, but by themselves not definitive, evidence for heterogeneous (e.g., nanoparticle) catalysis.[4b] Overall, the increased catalytic activity, color changes, and occasional bulk Ir(0) precipitate after the reaction require *at least one transformation processes of the catalyst, or possibly parallel development of different catalysts, during both the aging stage and the hydrogenation catalysis.* Nanocluster development is strongly implicated by just the color change, although verification of that by several independent methods quickly became the next objective.

The specific objectives for what follows, then, are (i) to determine the nuclearity of the Ir$_n$ species initially present and (ii) to determine the Ir$_n$ species present after the catalyst has entered the maximum rate regime. Those studies presented next comprise the first necessary step en route (iii) to determining the nature of the active catalyst during both the initial and the maximum rate regimes. An important additional goal is to (iv) determine to what extent the rate effect of different Al/Ir ratios is due to AlEt$_3$-induced changes in the initial Ir component of the catalyst (e.g., does Al/Ir influence initial Ir$_n$ nuclearity?) versus changes in just the AlEt$_3$-derived component. Additional studies concerning the challenging problem of the form(s) of the AlEt$_3$-derived species at varying Al/Ir ratios and their role in catalysis are necessarily addressed elsewhere.[13]

Tabulation of the Key Pre- and Posthydrogenation Catalyst Characterization. It will be easier to read what follows if we first summarize in Table 1 the key results from Z-contrast STEM, XAFS, and MALDI MS, both pre- and postcatalytic hydrogenation runs. The key findings will be that (i) a combination of the catalyst precursors [(1,5-COD)Ir(μ-O$_2$C$_8$H$_{15}$)]$_2$ and AlEt$_3$ gives catalytically active solutions containing a broad range of Ir$_n$ species spanning from monometallic Ir complexes to noncrystalline Ir$_n$ nanoclusters, with estimated mean 0.5−0.7 nm Ir$_{\sim4−15}$ clusters. However, (ii) after a catalytic run, the population of Ir$_n$ shifts considerably toward the form of approximately 1.0−1.6 nm, *fcc* Ir(0)$_{\sim40−150}$, Ziegler nanoclusters.

Nuclearity of the Ir$_n$ Species in Aged AlEt$_3$/Ir Catalyst *before* Hydrogenation: Z-Contrast Microscopy. A selected Z-contrast STEM image of a [(1,5-COD)Ir(μ-O$_2$C$_8$H$_{15}$)]$_2$ plus AlEt$_3$, Al/Ir = 2.0, catalyst sample, aged ≥2 days and analyzed *before* hydrogenation, shows clusters with a range of diameters, Figure 2. The size distribution histogram, also Figure 2, was constructed by measuring the full width at half-maximum (FWHM) of the intensity profile across 600 particles from images at the same levels of magnification and contrast. Most of the clusters counted in such images are subnanometer in scale. The mean cluster size is 0.5 ± 0.2 nm (a cluster 0.5 nm in diameter corresponds approximately to a theoretical tetrahedral Ir$_4$ cluster). The smallest Ir species observed appear to be mono-Ir complexes (diameter of Ir in a monometallic compound < 0.3 nm),[15] and the histogram

(15) Cordero, B.; Gómez, V.; Platero-Prats, A. E.; Revés, M.; Echeverría, J.; Cremades, E.; Barragán, F.; Alvarez, S. *Dalton Trans.* **2008**, 2832−2838.

Table 1. Observed Ir_n Cluster Diameters in the $[(1,5\text{-}COD)IrO_2C_8H_{15}]_2$ Catalyst Both Pre- and Post-Catalytic Runs by Three Different Analytical Methods

analytical method	precatalysis			postcatalysis		
	range (nm)	mean (nm)	mean Ir_n nuclearity	range (nm)	mean (nm)	mean Ir_n nuclearity
Z-Contrast STEM	0.2–1.4	0.5 ± 0.2	$Ir_{\sim 4}$	0.4–1.9	1.0 ± 0.3	$Ir_{\sim 40}$
XAFS	NA[a]	0.5	$Ir_{\sim 4}$	NA[a]	1.6	$Ir_{\sim 150}$
MALDI MS	0.5–1.1	0.7 ± 0.2[b]	$Ir_{\sim 15}$[b]	0.6–1.4	0.8 ± 0.2[b]	$Ir_{\sim 20}$[b]

[a] Determination of the range of Ir_n clusters present is not possible by this method. [b] An underestimate due to the irregular shape of the peak, which includes a high m/z tail (vide infra). See the discussion which follows for issues with the less reliable MALDI-MS in comparison to the Z-Contrast STEM and XAFS.
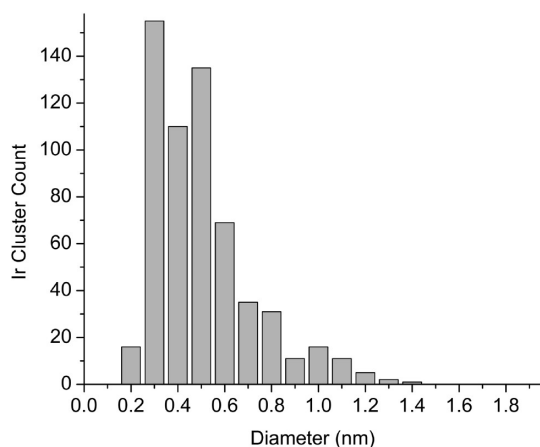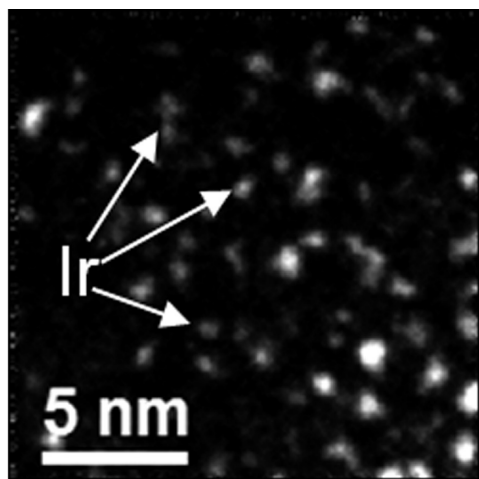
Figure 2. Representative Z-contrast STEM image of a $[(1,5\text{-}COD)Ir(\mu\text{-}O_2C_8H_{15})]_2$ plus $AlEt_3$ catalyst sample with an Al/Ir ratio of 2.0. Ir appears as white spots on a dark background. A diameter measurement of 600 clusters gives an overall distribution ranging from monometallic Ir complexes to 1.4 nm, $Ir_{\sim 100}$, clusters and a mean cluster diameter of 0.5 nm ($Ir_{\sim 4}$) ± 0.2 nm.

tails off toward larger Ir clusters present in much lower abundance, the largest observed being 1.4 nm in diameter $(Ir_{\sim 100})$.[16−18]

An Ir model Ziegler-type hydrogenation catalyst was chosen for the present studies in part because prior TEM

(16) Lin, Y.; Finke, R. G. *J. Am. Chem. Soc.* **1994**, *116*, 8335–8353.
(17) *CRC Handbook of Chemistry and Physics*, 77th ed.; Lide, D. R., Frederikse, H. P. R., Eds.; CRC Press: Boca Raton, FL, 1996.
(18) With the simplifying assumption of *fcc* clusters, the number (n) of atoms in a transition metal nanocluster of diameter D can be estimated according to $n = (N_0\rho(4/3)\pi(D/2)^3)/W$,[16] where $N_0 = 6.022 \times 10^{23}$ mol^{-1}, ρ = the room temperature density of the pure bulk metal, and W = atomic weight of the transition metal. For Ir, $\rho = 22.5$ g/cm^3 and $W = 192.22$ g/mol.[17] According to this estimate, the largest, 1.4-nm-diameter Ir clusters are $Ir(0)_{\sim 100}$.

experiments and controls have shown that the (third-row metal) Ir nanoclusters and precursor compounds generally have greater stability than lighter transition metal nanoclusters or precursors in TEM electron beams.[19−21] Moreover, it has been observed previously that at least first-row metal, Ni Ziegler-type hydrogenation catalysts are highly sensitive to sample preparation required by electron microscopy, specifically, the drying of catalyst samples on grids.[1] Z-contrast STEM cannot overcome the issue of sample drying but does offer the benefit of *scanning* TEM, so that potential sample damage can be minimized by using a small electron probe, low beam current, and minimum time of sample exposure to the electron beam.[22] In this case, the sizes and shapes of Ir spots in the images were continually monitored during image acquisition; no evidence of artifacts or modification of the sample as a result of the microscopy itself was observed, as expected for the third-row Ir system chosen in part for such superior TEM properties.[7a,16] In addition, *the greater resolving power of the Z-contrast method over conventional bright field TEM has permitted detection of the subnanometer clusters,*[22−25] which are important results. To summarize, Z-contrast microscopy indicates that aged catalyst samples before hydrogenation consist of a broad distribution of Ir_n species ranging from mono-Ir complexes to 1.4 nm, $Ir_{\sim 100}$ Ziegler nanoclusters. Significantly, subnanometer Ir_n clusters are the most abundant species present, and the mean Ir cluster diameter of 0.5 ± 0.2 nm corresponds to $Ir_{\sim 4}$ cluster compounds.

Identification of the Ir-Containing Species in Aged AlEt3/Ir Catalyst *before* Hydrogenation: XAFS Spectroscopy. XAFS data were first acquired for four reference

(19) Starkey Ott, L.; Cline, M. L.; Deetlefs, M.; Seddon, K. R.; Finke, R. G. *J. Am. Chem. Soc.* **2005**, *127*, 5758–5759.
(20) Hagen, C. M.; Vieille-Petit, L.; Laurenczy, G.; Süss-Fink; Finke, R. G. *Organometallics* **2005**, *24*, 1819–1831.
(21) Williams, D. B.; Carter, C. B. *Transmission Electron Microscopy*; Plenum Press: New York, 1996.
(22) Pyrz, W. D.; Buttrey, D. J. *Langmuir* **2008**, *24*, 11350–11360.
(23) Menard, L. D.; Gao, S.-P.; Xu, H.; Twesten, R. D.; Harper, A. S.; Song, Y.; Wang, G.; Douglas, A. D.; Yang, J. C.; Frenkel, A. I.; Nuzzo, R. G.; Murray, R. W. *J. Phys. Chem. B* **2006**, *110*, 12874–12883.
(24) The results of bright field TEM used to analyze the initial $[(1,5\text{-}COD)Ir(\mu\text{-}O_2C_8H_{15})]_2$ plus $AlEt_3$ catalyst samples, before their use in hydrogenation, are shown and discussed in the Supporting Information. An image obtained before hydrogenation of an Al/Ir = 2.0 catalyst sample shows 1.1 ± 0.3 nm diameter Ziegler nanoclusters. This larger mean diameter is a consequence of the inability of bright-field TEM to detect the ≤ ~1.0 nm Ir clusters. In addition, an image of the $[(1,5\text{-}COD)Ir(\mu\text{-}O_2C_8H_{15})]_2$ precatalyst alone as a control experiment contains dark spots that are likely artifacts of the image background. Hence, the bright-field TEM results were deemphasized in this study. HRTEM was also used to image catalyst samples before hydrogenation. However, images of reasonable quality were not obtained. A sample image and an explanation of the findings are given in the Supporting Information.
(25) Finney, E. E.; Finke, R. G. *J. Colloid Interface Sci.* **2008**, *317*, 351–374. Also see refs 45−49 therein.

samples: (i) an Ir black standard, (ii) HPO_4-stabilized *fcc* $Ir(0)_n$ nanoclusters,[26] (iii) $Ir_4(CO)_{12}$, and (iv) the precatalyst $[(1,5\text{-COD})Ir(\mu\text{-}O_2C_8H_{15})]_2$. XAFS data were then acquired for seven different samples of the initial, $[(1,5\text{-COD})Ir(\mu\text{-}O_2C_8H_{15})]_2$ plus $AlEt_3$ catalyst solutions aged ≥ 2 days, and before their use in hydrogenation: catalysts prepared with Al/Ir ratios of 0.5, 1.0, 1.5, 2.0, 2.5, 3.0, and 5.0. Six main results from the XAFS spectroscopy of aged catalyst samples *before hydrogenation* are that (i) all samples lack longer-range coordination shells (in r-space) that are characteristic of ordered nanoclusters. (ii) Spectra from the Al/Ir ≤ 1.0 samples are satisfactorily fit using a composite model created from an Ir–first-nearest-neighbor (hereafter 1NN) path from $[(1,5\text{-COD})Ir(\mu\text{-}O_2C_8H_{15})]_2$ and the Ir–Ir first-nearest-neighbor (1NN) single scattering path (hereafter SS1) from bulk Ir, but (iii) *modeling the Al/Ir ≥ 1.5 samples requires incorporating the contribution of the Ir–Al path*, an important finding. In addition, (iv) small Ir–Ir 1NN coordination numbers (*N*; roughly in the range of 2–3, vide infra) correspond to subnanometer Ir cluster sizes. (v) Ir–Ir 1NN distances longer than expected for bulk Ir or ordered Ir nanoclusters indicate valence-electron sharing with ligands, consistent with small, ligated molecular Ir clusters, and (vi) XANES spectra of the Ir catalyst samples differ from bulk Ir but are similar to the precursor $[(1,5\text{-COD})Ir(\mu\text{-}O_2C_8H_{15})]_2$ and $Ir_4(CO)_{12}$, suggesting formally $Ir(I)_n$ or $Ir(0)_n$ molecular clusters of few Ir atoms ligated by relatively strongly electron-withdrawing groups. The only sources of ligands in the system other than the weakly coordinating cyclohexane solvent are $AlEt_3$, $C_7H_{15}CO_2^-$, and possibly Ir–H (given that the 1,5-COD is hydrogenated to cyclooctane in the reaction), so that the list of possible, dominant species present that could be ligands is actually rather short, primarily, $AlEt_3$, $C_7H_{15}CO_2AlEt_3^-$, and possibly Ir–H–$AlEt_3$ (among a few others such as any Al–O–Al containing alumoxanes formed by trace water present, water that our experimental efforts and conditions have strived to minimize; see the Experimental Section). In short, the XAFS studies reveal that *initial catalyst* solutions lack ordered $Ir(0)_n$ nanoclusters and contain, on average, molecular $Ir_{\sim 4}$, 0.5 nm clusters ligated by electron-withdrawing groups that are likely derived from the short list of ligands listed above.

Fourier transform (FT) magnitudes of the background-subtracted XAFS signals for the Al/Ir-dependent sample series are shown in Figure 3. FT magnitude data of selected reference samples and a catalyst sample with an Al/Ir ratio of 2.0 are shown together in Figure 4. For single scattering paths (SS1, SS2, etc.), the positions of isolated peaks in FT plots correspond to the distance between the absorber and its neighbors, albeit shorter than the actual distances due to the photoelectron phase shifts.[27−29] The first important observation is that in the FT magnitude sample spectra, Figure 3, there is a lack of
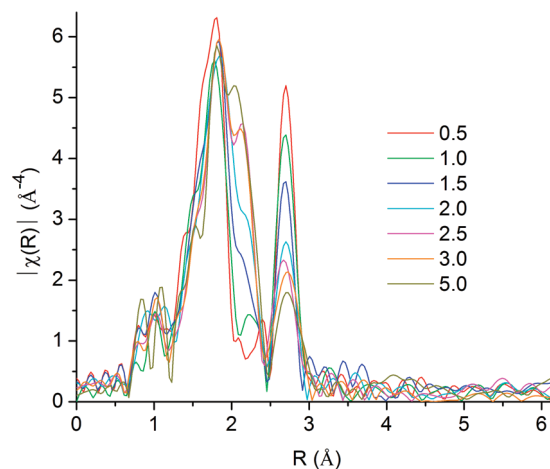
Figure 3. A k^3-weighted FT magnitude plot of a series of catalyst samples made from the combination of $[(1,5\text{-COD})Ir(\mu\text{-}O_2C_8H_{15})]_2$ and $AlEt_3$ (Al/Ir = 0.5, 1.0, 1.5, 2.0, 2.5, 3.0, 5.0) before their use in hydrogenation. The lack of peaks in the 3–6 Å region indicates the absence of crystalline Ir particles. The large peak on the left at ~1.8 Å represents Ir–C and/or Ir–O backscattering contributions (hereafter, "Ir–X", since XAFS cannot distinguish between C and O backscatterers in catalyst samples, vide infra). The shoulder at ~2.2 Å on the right of the larger, Ir–X peak that grows in with increasing Al/Ir ratio is well-modeled by single scattering due to Al atoms. The narrow peak at ~2.7 Å represents single scattering from the first Ir–Ir nearest neighbor shell. *R* values are uncorrected for photoelectron phase shifts.
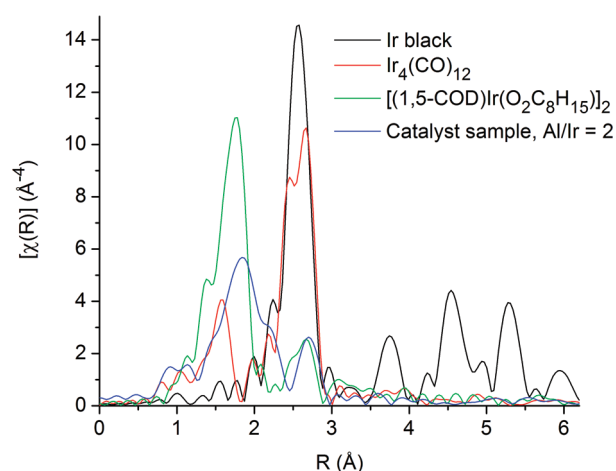
Figure 4. A plot of FT magnitude of the k^3-weighted XAFS data for Ir black (scaled by 1/4 for ease of comparison), $Ir_4(CO)_{12}$ (scaled by 1/2 for ease of comparison), $[(1,5\text{-COD})Ir(\mu\text{-}O_2C_8H_{15})]_2$, and a catalyst sample, with an Al/Ir of 2.0, for comparison. The peaks in the 3–6 Å range, seen here only in the spectrum of Ir black, are diagnostic of an ordered Ir phase.

distinct peaks in the 3−6 Å range expected for SS2−5 paths, whereas such peaks are visible in the FT magnitude plots of Ir black, Figure 4 and Figure S10, Supporting Information. The lack of these peaks indicates that before hydrogenation there is not an appreciable amount of Ir nanoclusters with ordered, periodic, atomic structures in the catalyst. Restated, the *aged catalyst sample before hydrogenation lacks the XAFS longer r-range contribution expected if ordered nanoclusters were present.* Hence, the relatively few nanometer-sized clusters that are present before hydrogenation according to Z-contrast STEM (as well as bright field TEM; see the Supporting Information) appear to have significantly *disordered atomic structures*

(26) (a) Özkar, S.; Finke, R. G. *J. Organomet. Chem.* **2004**, *689*, 493–501. (b) Özkar, S.; Finke, R. G. *Langmuir* **2003**, *19*, 6247–6260.

(27) Frenkel, A. I.; Hills, C. W.; Nuzzo, R. G. *J. Phys. Chem. B* **2001**, *105*, 12689–12703.

(28) In *X-ray Absorption: Principles, Applications, Techniques of EXAFS, SEXAFS, and XANES*; Koningsberger, D. C., Prins, R., Eds.; Wiley: New York, 1988.

(29) Stern, E. A.; Heald, S. M. In *Handbook on Synchrotron Radiation*; Koch, E. E., Ed.; North-Holland: New York, 1983; Vol. *1*.

(this finding and its significance are discussed in further detail below).[30−37]

Fitting Results for Catalyst Samples before Hydrogenation. XAFS spectra of Ir black, HPO_4-stabilized *fcc* Ir(0) nanoclusters, $Ir_4(CO)_{12}$, and $[(1,5-COD)Ir(\mu-O_2C_8H_{15})]_2$ were fit using theoretical models based on the crystal structures of bulk *fcc* Ir, $Ir_4(CO)_{12}$,[38] and $[(1,5-COD)Ir-(\mu-O_2C_8H_{15})]_2$, respectively.[2] Fits of these standards and reference compounds are shown in Figures S10−S14, Supporting Information, and the fitting results are summarized in Tables S1−S5, Supporting Information, for the interested reader. The peaks in the spectra of $Ir_4(CO)_{12}$ and $[(1,5-COD)Ir(\mu-O_2C_8H_{15})]_2$ at about 1.6 Å and 1.8 Å, Figure 4, correspond to Ir−C and Ir−X first nearest neighbors (again abbreviated 1NN), respectively (X represents both C and O atoms, which were nondistinguishable by XAFS in $[(1,5-COD)Ir(\mu-O_2C_8H_{15})]_2$, Figure S13, Supporting Information, and in the catalyst samples). The peaks in the spectra of Ir black, HPO_4-stabilized Ir nanoclusters and $Ir_4(CO)_{12}$ at about 2.5 Å correspond to Ir−Ir 1NN positions. Comparing the spectra in Figures 3 and 4, the peaks in the catalyst samples near 1.8 Å and 2.7 Å correspond, roughly, to scattering contributions from Ir−X and Ir−Ir, respectively. Therefore, scattering

Figure 5. FT magnitude spectra and fits for the Al/Ir = 1.0 (a) and 2.0 (b) catalysts. The model used to fit the Al/Ir = 1.0 sample was created from the Ir−X path in $[(1,5-COD)Ir(\mu-O_2C_8H_{15})]_2$ and the Ir−Ir SS1 path in Ir black. The Al/Ir = 2.0 sample was fit by the same model but modified to account for backscattering by Al atoms in close proximity to the absorbing Ir.

paths for Ir−X and Ir−Ir were used to model the catalyst sample data.

Fits of the catalyst sample data using a model created from the Ir−X path in $[(1,5-COD)Ir(\mu-O_2C_8H_{15})]_2$ and the Ir−Ir SS1 path in Ir black gave physically reasonable results only for the Al/Ir = 0.5 and 1.0 samples. For the Al/Ir ≥ 1.5 samples, the model was adapted by taking into account backscattering by Al atoms in close proximity to the absorbing Ir. This modified model better accounted for the shoulder on the right side of the leftmost (Ir−X) peak that grows in with the 1.5 and higher Al/Ir ratio samples, Figure 3. However, attempts to use the model incorporating Al to fit the Al/Ir = 0.5 and 1.0 sample data gave unreasonable results. Fits to the Al/Ir = 1.0 and 2.0 sample data using the model that neglects Al and the model that incorporates Al, respectively, are shown in Figure 5. The fitting results for all samples are summarized in Table 2. Additional spectra of the data and theoretical fits are shown in Figures S15−S21, Supporting Information.

From the fit of the Al/Ir = 2.0 sample data, the 1NN Ir−Ir N of 3 ± 1 indicates an $Ir_{\sim4}$ cluster, which, in turn, corresponds to an Ir cluster roughly 0.5 nm in diameter. Results for catalyst samples at all $AlEt_3$/Ir ratios tested *are similar*, giving subnanometer, $Ir_{\sim4}$, clusters. Significantly, *XAFS and Z-contrast microscopy fortify one another in finding the same mean cluster size within experimental error.* Recall that Z-contrast

(30) The atomic-scale structure of transition metal nanoclusters is a topic of interest in the literature.[31−34] Theoretical and experimental studies have predicted and observed, respectively, the internal atomic structures of transition metal clusters from a variety of different systems,[31] including supported clusters.[32] It is found from such studies that nanoscale clusters can possess an assortment of internal structures and exhibit large degrees of structural disorder, or an amorphous-like nature, even while maintaining some signatures of periodicity.[31f] However, precise determination of the internal atomic structures on the nanoscale is a nontrivial problem,[33] especially since examples of systems that are amenable to such structural analysis are rare.[34]

(31) (a) Duff, D. G.; Curtis, A. C.; Edwards, P. P.; Jefferson, D. A.; Johnson, B. F. G.; Logan, D. E. *J. Chem. Soc., Chem. Commun.* **1987**, 1264–1266. (b) Ankudinov, A. L.; Rehr, J. J.; Low, J. J.; Bare, S. R. *J. Chem. Phys.* **2002**, *116*, 1911–1919. (c) Garzón, I. L.; Reyes-Nava, J. A.; Rodríguez-Hernández, J. I.; Sigal, I.; Beltrán, M. R; Michaelian, K. *Phys. Rev. B* **2002**, *66*, 073403–1−073403–4. (d) Petkov, V.; Ohta, T.; Hou, Y.; Ren, Y. *J. Phys. Chem. C* **2007**, *111*, 714–720. (e) Sanchez, S. I.; Small, M. W.; Zuo, J.-M.; Nuzzo, R. G. *J. Am. Chem. Soc.* **2009**, *131*, 8683–8689. (f) Petkov, V.; Bedford, N.; Knecht, M. R.; Weir, M. G.; Crooks, R. M.; Tang, W.; Henkelman, G.; Frenkel, A. *J. Phys. Chem. C* **2008**, *112*, 8907–8911. (g) Sun, Y.; Zhuang, L.; Lu, J.; Hong, X.; Liu, P. *J. Am. Chem. Soc.* **2007**, *129*, 15465–15467. Interestingly these authors also see that larger (Pt) nanoparticles have an increased activity, and that the smaller ≤1 nm Pt nanoparticles are amorphous (perhaps due to Pt−O or other surface ligands).

(32) (a) Vila, F.; Rehr, J. J.; Kas, J.; Nuzzo, R. G.; Frenkel, A. I. *Phys. Rev. B* **2008**, *78*, 121404−1–121404−4. (b) Sanchez, S. I.; Menard, L. D.; Bram, A.; Kang, J. H.; Small, M. W.; Nuzzo, R. G.; Frenkel, A. I. *J. Am. Chem. Soc.* **2009**, *131*, 7040–7054.

(33) (a) Gilbert, B.; Huang, F.; Zhang, H.; Waychunas, G. A.; Banfield, J. F. *Science* **2004**, *305*, 651–654. (b) Billinge, S. J. L.; Levin, I. *Science* **2007**, *316*, 561–565.
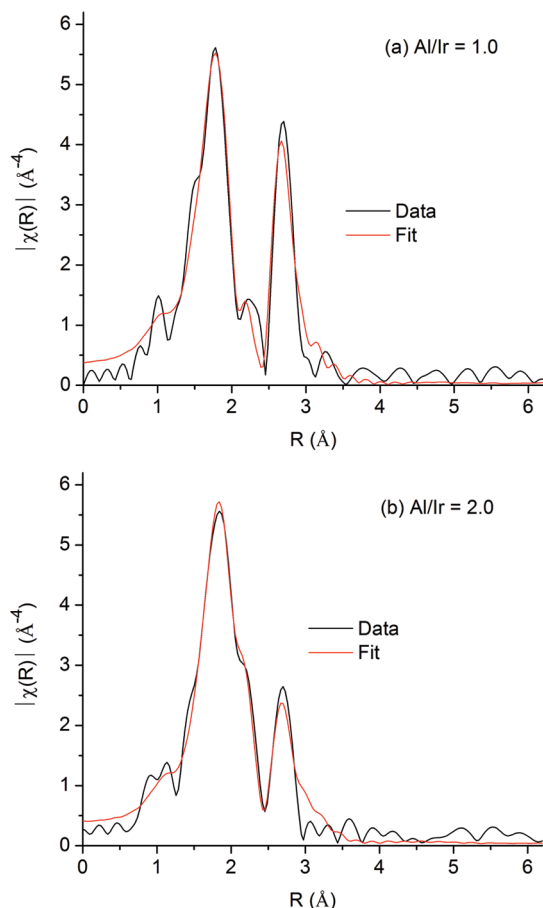
(34) Jadzinsky, P. D.; Calero, G.; Ackerson, J. C.; Bushnell, D. A.; Kornberg, R. D. *Science* **2007**, *318*, 430–433.

(35) (a) Sun, Y.; Frenkel, A. I.; Isseroff, R.; Shonbrun, C.; Forman, M.; Shin, K.; Koga, T.; White, H.; Zhang, L.; Zhu, Y.; Rafailovich, M. H.; Sokolov, J. C. *Langmuir* **2006**, *22*, 807–816. (b) Menard, L. D.; Xu, H.; Gao, S.-P.; Twesten, R. D.; Harper, A. S.; Song, Y.; Wang, G.; Douglass, D.; Yang, J. C.; Frenkel, A. I.; Murray, R. W.; Nuzzo, R. G. *J. Phys. Chem. B* **2006**, *110*, 14564–14573. (c) Soler, J. M.; Beltrán, M. R.; Michaelian, K.; Garzón, I. L.; Ordejón, P.; Sánchez-Portal, D.; Artacho, E. *Phys. Rev. B* **2000**, *61*, 5771–5780.

(36) Fulton, J. L.; Linehan, J. C.; Autrey, T.; Balasubramanian, M.; Chen, Y.; Szymczak, N. K. *J. Am. Chem. Soc.* **2007**, *129*, 11936–11949.

(37) Harada, M; Asakura, K.; Toshima, N. *J. Phys. Chem.* **1994**, *98*, 2653–2662.

(38) Churchill, M. R.; Hutchinson, J. P. *Inorg. Chem.* **1978**, *17*, 3528–3535.

Table 2. Fitting Results for the [(1,5-COD)Ir(μ-O$_2$C$_8$H$_{15}$)]$_2$ Plus AlEt$_3$ Catalyst Samples before Their Use in Hydrogenation

sample Al/Ir	Ir black	0.5	1.0	1.5	2.0	2.5	3.0	5.0
$N_{\text{Ir}-\text{Ir}}$	12^c	1.8 ± 0.4	2.8 ± 0.6	2.1 ± 0.6	3 ± 1	3 ± 1	3 ± 1	3 ± 3
$N_{\text{Ir}-\text{X}}$		6.0 ± 0.6	5.8 ± 0.6	5.4 ± 0.8	5.0 ± 0.7	4.7 ± 0.8	4.8 ± 0.8	5 ± 1
$N_{\text{Ir}-\text{Al}}$				1.0 ± 0.9	1.7 ± 0.8	2 ± 1	3 ± 1	3 ± 2
$R_{\text{Ir}-\text{Ir}}$ (Å)^a	2.711 ± 0.001	2.799 ± 0.005	2.797 ± 0.005	2.803 ± 0.007	2.826 ± 0.007	2.84 ± 0.01	2.849 ± 0.008	2.86 ± 0.02
$R_{\text{Ir}-\text{X}}$ (Å)^a		2.149 ± 0.007	2.162 ± 0.008	2.18 ± 0.01	2.19 ± 0.01	2.19 ± 0.02	2.19 ± 0.01	2.20 ± 0.03
$R_{\text{Ir}-\text{Al}}$ (Å)^a				2.49 ± 0.02	2.51 ± 0.01	2.51 ± 0.01	2.51 ± 0.01	2.5045^c
$\sigma^2_{\text{Ir}-\text{Ir}}$ (Å^2)^b	3.5 ± 0.1	5.2 ± 0.7	7.0 ± 0.7	7 ± 1	10 ± 1	10 ± 2	10 ± 2	11 ± 4
$\sigma^2_{\text{Ir}-\text{X}}$ (Å^2)^b		6.4 ± 0.9	8 ± 1	7 ± 1	7 ± 1	8 ± 2	8 ± 1	9 ± 3
$\sigma^2_{\text{Ir}-\text{Al}}$ (Å^2)^b				7 ± 5	8 ± 3	8 ± 2	8 ± 3	8 ± 4

^{a} R is the experimentally determined interatomic distance for the Ir–X, Ir–Al, and Ir–Ir single scattering paths. ^{b} σ^2, the Debye–Waller factor, is the mean square variation in R due to static and dynamic disorder. The values shown are $\times 10^3$. ^{c} For this sample only, this parameter was defined to be the value shown and not varied in the fit.

STEM also reveals a broad dispersity of Ir cluster sizes in catalyst samples before hydrogenation. XAFS, on the other hand, gives ensemble-average results for local structure; it does *not* provide information regarding *distribution* of Ir cluster sizes.[35] In light of the larger clusters observed by electron microscopy (the tail in the histogram of Figure 2 showing some Ir$_n$ clusters with nanometer scale diameters), possible explanations for the XAFS results are that the nanoscale Ir clusters could (i) have considerably disordered structures,[31] (ii) actually be groups of tightly associated Ir$_{\sim 4}$ clusters that also exist in solution,[36,37] or (iii) simply be artifacts brought about by the ex situ technique itself, with the ex situ observed clusters not existing in the solutions used in cyclohexene hydrogenation and examined by XAFS spectroscopy. However, the similar Ir cluster sizes and distributions obtained by *both* Z-contrast STEM and MALDI MS (vide infra), and the XAFS-determined Ir–Ir bond lengths and bond length disorders larger than those observed in bulk Ir (see Table 2, and the text below), make the *presence* of highly disordered nanoscale Ir clusters—along with a majority of subnanometer, Ir$_{\sim 4}$ clusters—a preferred explanation. The key finding by XAFS, then, is that *initial, precatalytic hydrogenation solutions are composed, on average, of Ir$_{\sim 4}$, 0.5 nm clusters.*

Significantly, the R values for Ir–Ir 1NNs in all samples are *larger* than the theoretical values from bulk Ir, Table 2. If transition metal nanoclusters were the dominant species present, then the M–M distances should have been *smaller* (and as we will see posthydrogenation, vide infra), distances contracted in order to minimize the surface free energy (the surface free energy of small metal clusters is elevated due to the unsatisfied bonding requirements and too-low coordination number of the surface metals).[31,39] However, the observed, longer Ir–Ir distances are fully consistent with subnanometer, Ir$_{\sim 4}$ cluster compounds[36,40–42] coordinated to any available ligands such as those listed earlier, namely, AlEt$_3$, C$_7$H$_{15}$CO$_2$-AlEt$_3^-$, and possibly Ir–H–AlEt$_3$. The possibility of Ir–Al bonding (or possibly Ir–X–Al, X = H or Et, bonding) is consistent with the XAFS data; fits of samples with Al/Ir ratios from 1.5–3.0 reveal Al at a distance from Ir of 2.5 Å, which is within the range found for

γ-Al$_2$O$_3$-supported Ir$_4$ and Ir$_6$ clusters.[43] Additionally, the Ir to Al atom-pair distance of ca. 2.5 Å obtained by XAFS is close to crystallographically determined distances 2.456(1) Å and 2.459(1) Å in (Cp*(PMe$_3$)IrAl-Et)$_2$, which possesses an Ir–Al–Ir bridging motif but is shorter than the Ir–H–Al bond distance of 2.684(2) in Cp*(PMe$_3$)Ir(H)$_2$AlPh$_3$.[44] These results are of considerable significance in addressing likely ligands derived from the AlEt$_3$ and C$_7$H$_{15}$CO$_2^-$ components of the catalyst, and under the reaction conditions.[13]

The three main results from fitting the XAFS spectra, then, are (i) samples with Al/Ir ratios ≥1.5 are best fit using a model incorporating backscattering from Al; (ii) low Ir–Ir first-nearest neighbor coordination numbers imply, on average, Ir$_{\sim 4}$, 0.5 nm clusters; (iii) Ir–Ir distances longer than expected for bulk Ir were found, consistent with Ir ligated by the ligands present in species such as Ir–X–Al or possible direct Ir–Al interaction. Significantly, the Z-contrast STEM and XAFS results *are consistent, giving Ir$_{\sim 4}$, 0.5 nm clusters as the mean Ir$_n$ clusters.* The identical mean cluster size results from Z-contrast STEM and XAFS argue strongly against artifacts introduced by either method, including the ex situ STEM, which in turn suggests that the *Ir$_{\sim 4}$, 0.5 nm clusters are, as the Z-contrast STEM reveals, a major part of a broad distribution of Ir$_n$ clusters.*

The X-ray absorption near-edge structure (XANES) was used to probe the oxidation state of the initial catalyst solutions. The XANES regions of Ir black, Ir$_4$(CO)$_{12}$, and [(1,5-COD)Ir(μ-O$_2$C$_8$H$_{15}$)]$_2$ are shown in Figure 6 alongside those for the Al/Ir = 1.0 and 2.0 catalyst samples before hydrogenation. The XANES spectra of the catalyst samples are similar to the [(1,5-COD)Ir(I)(μ-O$_2$C$_8$H$_{15}$)]$_2$ precursor and Ir(0)$_4$(CO)$_{12}$ standard (formally Ir(I) and Ir(0), respectively) but unlike the Ir(0) black standard. This is the case regardless of the Al/Ir ratio of the sample and suggests that the Ir species present are formally Ir(I) or Ir(0) ligated by the previously listed ligand possibilities.

A sample of the [(1,5-COD)Ir(μ-O$_2$C$_8$H$_{15}$)]$_2$ plus AlEt$_3$ catalyst, Al/Ir of 2.0, was analyzed by XPS to distinguish whether the Ir species in the catalyst before hydrogenation are Ir(I) or Ir(0); experimental XPS spectra and literature reference data are given in the Supporting Information. The Ir 4f peak positions at 64.30 and 61.33 eV in the experimental

(39) Finke, R. G.; Özkar, S. *Coord. Chem. Rev.* **2004**, *248*, 135–146.

(40) Shido, T.; Okazaki, T.; Ichikawa, M. *J. Mol. Catal. A: Chem.* **1997**, *120*, 33–45.

(41) Cho, S. J.; Lee, J.; Lee, Y. S.; Kim, D. P. *Catal. Lett.* **2006**, *109*, 181–187.

(42) Garlaschelli, L.; Greco, F.; Peli, G.; Manassero, M.; Sansoni, M.; Gobetto, R.; Salassa, L.; Pergola, R. D. *Eur. J. Inorg. Chem.* **2003**, 2108–2112.

(43) Argo, A. M.; Odzak, J. F.; Gates, B. C. *J. Am. Chem. Soc.* **2003**, *125*, 7107–7115.

(44) Golden, J. T.; Peterson, T. H.; Holland, P. L.; Bergman, R. G.; Andersen, R. A. *J. Am. Chem. Soc.* **1998**, *120*, 223–224.
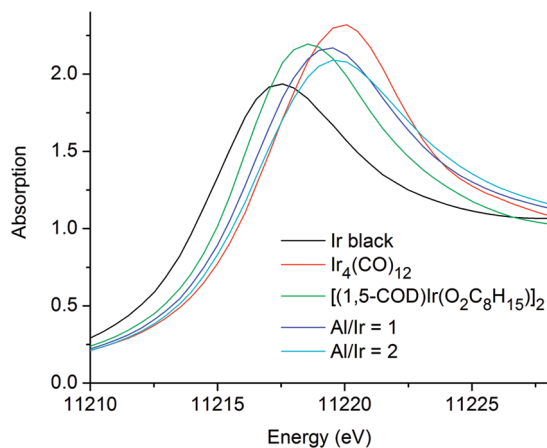
Figure 6. XANES portions of the normalized $\mu(E)$ spectra for Ir black (black line), $Ir_4(CO)_{12}$ (red), the $[(1,5\text{-COD})Ir(\mu\text{-}O_2C_8H_{15})]_2$ precatalyst (green), and the $AlEt_3/Ir$ = 1.0 and 2.0 samples before hydrogenation (blue and light blue). The catalyst samples before hydrogenation are comparable to the formally Ir(I) and Ir(0) $[(1,5\text{-COD})Ir(\mu\text{-}O_2C_8H_{15})]_2$ precatalyst and $Ir_4(CO)_{12}$ standard, respectively.

XPS spectrum can be attributed to Ir(I)[45] but are also consistent with (i.e., indistinguishable from) $Ir(0)_n$ Ziegler nanoclusters exhibiting a final-state relaxation effect.[46−53] Therefore, both XANES and XPS results of catalyst samples before their use in hydrogenation are consistent with Ir(I) species as well as $Ir(0)_n$ Ziegler nanoclusters (or both), but cannot unambiguously distinguish these.

To summarize the observations from XAFS spectroscopy on the aged catalyst samples, but before hydrogenation, (i) longer range scattering peaks, expected for ordered nanoclusters, are not seen; (ii) successful fitting of the Al/Ir ≥ 1.5 catalyst sample spectra requires a model that includes the backscattering from Al atoms in close proximity to Ir atoms; (iii) small Ir−Ir N values are obtained that correspond to subnanometer cluster sizes; (iv) Ir−Ir bonds longer than expected for bulk or $Ir(0)_n$ nanoclusters, but consistent with ligated $Ir_{\sim4}$ subnanometer clusters, are seen; (v) XANES spectra are different than those of bulk Ir but are comparable to the $[(1,5\text{-COD})Ir(\mu\text{-}O_2C_8H_{15})]_2$ precursor and $Ir_4(CO)_{12}$. These observations suggest that the initial catalyst samples, regardless of the Al/Ir ratio, are composed on average of Ir(I) or Ir(0) subnanometer, molecular $Ir_{\sim4}$ clusters shielded from agglomeration by coordinated ligands.[54−59] The observations made here by XAFS on catalyst *solutions* are also fully consistent with and supported by the results from (the ex situ, solid state) Z-contrast STEM, which indicates that catalyst samples before hydrogenation are composed of a broad range of cluster sizes from mono-Ir molecules to nanometer scale noncrystalline Ir_n clusters, the most abundant being sub-nanometer Ir clusters, and the mean clusters being $Ir_{\sim4}$, 0.5 nm. The use of these complementary methods and their agreement is important; the results argue strongly against significant sample preparation and method-specific (and ex-situ versus in situ) artifacts. The results confirm our design criteria of using the more-stable, third-row Ir precatalyst (i.e., with its stronger Ir−Ir bonds and resultant greater cluster and nanocluster stability) as a needed, but previously little investigated, Ziegler-type hydrogenation catalyst model system.

Nuclearity of the Ir_n Species in $AlEt_3/Ir$ Catalyst *before* Hydrogenation: MALDI MS. Despite the agreement between the Z-contrast STEM and XAFS results, an additional method was used in order to further probe the Ir_n cluster size and distribution—as well as to "calibrate" that matrix assisted laser desorption ionization mass spectrometry (MALDI MS) method in this instance; is this ex-situ method reliable? Initial catalyst samples, before their use in hydrogenation but without aging, were analyzed. The experimental methods are discussed in greater detail in the Supporting Information for the interested reader, and spectra are shown there as well. Briefly, the ex situ MALDI MS on dried, solid samples reveals a broad Ir-containing peak centered at about 2800 m/z. The FWHM ranges from 1000−5000 m/z, and the peak tails off toward the higher m/z values. With the necessary *assumptions* that the broad peak observed in the full mass spectrum is composed of only

(45) El-Issa, B. D.; Katrib, A.; Ghodsian, R.; Salsa, B. A.; Addassi, S. H. *Int. J. Quantum Chem.* **1988**, *33*, 195–216.

(46) According to the final-state-relaxation phenomenon, electron photoemission results in a positive charge on the nanocluster surface, which has a lifetime longer than the time scale of the photoemission (10^{-16} s). This results in an electron binding energy that is shifted higher by 0.1−2.0 eV. The final state relaxation phenomenon has been previously observed for Au_n,[47,53] Pt_n,[48,49,51,52] and Pd_n,[52] nanoclusters 1−10 nm in diameter. Therefore, the ~0.5 eV positive shift of the Ir 4f peaks in the experimental XPS spectrum (at 64.30 and 61.33 eV) with respect to literature values for bulk Ir(0) could be explained by the final state relaxation effect.

(47) Wertheim, G. K.; DiCenzo, S. B.; Youngquist, S. E. *Phys. Rev. Lett.* **1983**, *51*, 2310–2313.

(48) Fu, X.; Wang, Y.; Wu, N.; Gui, L.; Tang, Y. *J. Colloid Interface Sci.* **2001**, *243*, 326–330.

(49) Tu, W.; Takai, K.; Fukui, K.; Miyazaki, A.; Enoki, T. *J. Phys. Chem. B* **2003**, *107*, 10134–10140.

(50) De Heer, W. A. *Rev. Mod. Phys.* **1993**, *65*, 611–676.

(51) Eberhardt, W.; Fayet, P.; Cox, D. M.; Fu, Z.; Kaldor, A.; Sherwood, R.; Sondricker, D. *Phys. Rev. Lett.* **1990**, *64*, 780–783.

(52) Cheung, T. T. P. *Surf. Sci.* **1984**, *140*, 151–164.

(53) Ohgi, T.; Fujita, D. *Phys. Rev. B* **2002**, *66*, 115410.

(54) The formally Ir(I) "$[(1,5\text{-COD})IrH]_4$" is one reasonable hypothesis for an actual form of initial "Ir_4" species in this system consistent with the XANES spectra and XPS results (both methods being unable to distinguish unambiguously whether the mean $Ir_{\sim4}$, 0.5 nm species by XAFS is Ir(I) or Ir(0)). In fact, the previously unknown $[(1,5\text{-COD})Ir(\mu\text{-H})]_4$ has recently been prepared[13] by us by analogy to the synthesis for the known, formally Rh(I) compound, $[(1,5\text{-COD})RhH]_4$.[55] Other known "Ir_4H_x" species are $[(\eta^5\text{-}C_5Me_5Ir)_4H_4](BF_4)_2$[56] and $[Ir_4H_8(CO)_4(PPh_3)_4]$.[42] Additionally, M_4H_4-type clusters have been of interest as catalysts (or catalyst precursors) in other systems, often with the metal being Ru or Os.[56,57] Noteworthy here is that the formation,[58] and hydrogenation activity,[59] of oxide-supported, tetrahedral Ir_4 clusters have been studied extensively by Gates and co-workers.

(55) (a) Kulzick, M.; Price, R. T.; Muetterties, E. L.; Day, V. W. *Organometallics* **1982**, *1*, 1256–1258. (b) Duan, Z.; Hampden-Smith, M. J. *Chem. Mater.* **1992**, *4*, 1146–1148.

(56) Cabeza, J. A.; Nutton, A.; Mann, B. E.; Brevard, C.; Maitlis, P. M. *Inorg. Chim. Acta* **1986**, *115*, L47–L48.

(57) (a) Frediani, P; Matteoli, U.; Bianchi, M.; Piacenti, F.; Menchi, G. *J. Organomet. Chem.* **1978**, *150*, 273–278. (b) Bradley, J. S. *J. Am. Chem. Soc.* **1979**, *101*, 7419–7421. (c) Doi, Y.; Koshizuka, K.; Keii, T. *Inorg. Chem.* **1982**, *21*, 2732–2736. (d) Doi, Y.; Tamura, S.; Koshizuka, K. *J. Mol. Catal.* **1983**, *19*, 213–222. (e) Sánchez-Delgado, R. A.; Andriollo, A.; Puga, J.; Martín, G. *Inorg. Chem.* **1987**, *26*, 1867–1870. (f) Bhaduri, S.; Sharma, K. *J. Chem. Soc., Chem. Commun.* **1988**, 173–174. (g) Bhaduri, S.; Sharma, K.; Mukesh, D. *J. Chem. Soc., Dalton Trans.* **1992**, 77–81. (h) Adams, R. D.; Falloon, S. B. *Organometallics* **1995**, *14*, 4594–4600.

(58) (a) Goellner, J. F.; Guzman, J.; Gates, B. C. *J. Phys. Chem. B* **2002**, *106*, 1229–1238. (b) Li, F.; Gates, B. C. *J. Phys. Chem. B* **2003**, *107*, 11589–11596. (c) Li, F.; Gates, B. C. *J. Phys. Chem. B* **2004**, *108*, 11259–11264. (d) Uzun, A.; Gates, B. C. *Angew. Chem., Int. Ed.* **2008**, *47*, 9245–9248.

(59) (a) Xu, Z.; Xiao, F.- S.; Purnell, S. K.; Alexeev, O.; Kawi, S.; Deutsch, S. E.; Gates, B. C. *Nature* **1994**, *372*, 346–348. (b) Argo, A. M.; Odzak, J. F.; Lai, F. S.; Gates, B. C. *Nature* **2002**, *415*, 623–626.

Ir atoms[60−62] and that the ionic charges are $+1$,[60,62,63] the peak maximum corresponds to Ir$_{\sim15}$, 0.7-nm-diameter clusters.[18] Likewise, the FWHM of the peak corresponds to Ir$_{\sim5-26}$, 0.5−0.9-nm-diameter clusters (used to estimate the mean Ir$_n$ cluster size at 0.7 ± 0.2 nm), and the high m/z tail gives an indication of larger clusters present in relatively low numbers. The high m/z tail at one-fourth maximum intensity of the broad peak is positioned at 6000 m/z, which corresponds to Ir$_{\sim30}$, 0.9−1.0 nm clusters. The high m/z region of the spectrum continues to tail off, indicating the presence of Ir nanoclusters, but in a much lower abundance—for example, Ir$_{\sim50}$, 1.1-nm-diameter clusters at one-eighth the maximum peak intensity (and used as the maximum range limit reported in Table 1).

The quite different MALDI MS method proved useful in that it provides independent evidence for *similar* (albeit not identical) sizes and size distributions of Ir$_n$ clusters. The difference between the *estimated* mean Ir$_{\sim15}$, 0.7 nm clusters from MALDI MS and the mean Ir$_{\sim4}$, 0.5 nm clusters indicated by both Z-contrast STEM and XAFS may be the result of (i) factors due to the differences of the methods, (ii) imperfection in the assumptions necessary for this interpretation of MALDI MS, (iii) the fact that the sample analyzed by MALDI MS was not aged whereas the Z-contrast STEM and XAFS samples were aged; or (iv) some combination thereof. Regardless, the significance here is that MALDI MS confirms, in general, the results of Z-contrast STEM by giving independent evidence that the [(1,5-COD)Ir(μ-O$_2$-C$_8$H$_{15}$)]$_2$ plus AlEt$_3$ catalyst sample, with an Al/Ir ratio of 2.0, *before* hydrogenation, is composed of a broad distribution of Ir$_n$ clusters, which are primarily subnanometer Ir$_n$ clusters, but include, to a lesser extent, Ir$_n$ nanoclusters. The generally similar results argue against *significant* artifacts caused by these three very different physical methods. The main point is that in catalyst samples before hydrogenation there is a distribution in Ir$_n$ species centered on subnanometer Ir$_n$ clusters, and that the *estimated* mean cluster sizes are 0.5−0.7 nm, Ir$_{\sim4-15}$.

Identification of the Ir-Containing Species in the AlEt$_3$/Ir Catalyst *after* Hydrogenation: Z-Contrast and HRTEM Microscopy. The size and size distribution of Ir clusters, in a [(1,5-COD)Ir(μ-O$_2$C$_8$H$_{15}$)]$_2$ plus AlEt$_3$ catalyst sample with an Al/Ir ratio of 2.0 and *after* its use for cyclohexene hydrogenation, were analyzed using Z-contrast microscopy. Sample Z-contrast images and a histogram are shown in Figure 7. Measurement of 635 Ir clusters resulted in a mean diameter of 1.0 ± 0.3 nm, with observed Ir$_n$ cluster diameters spanning from 0.4 to 1.9 nm (two additional Ir nanoclusters, with larger diameters of 3.1 and 3.8 nm, were also observed).

Also obtained were HRTEM images of [(1,5-COD)Ir(μ-O$_2$C$_8$H$_{15}$)]$_2$ plus AlEt$_3$ catalyst samples after hydrogenation,
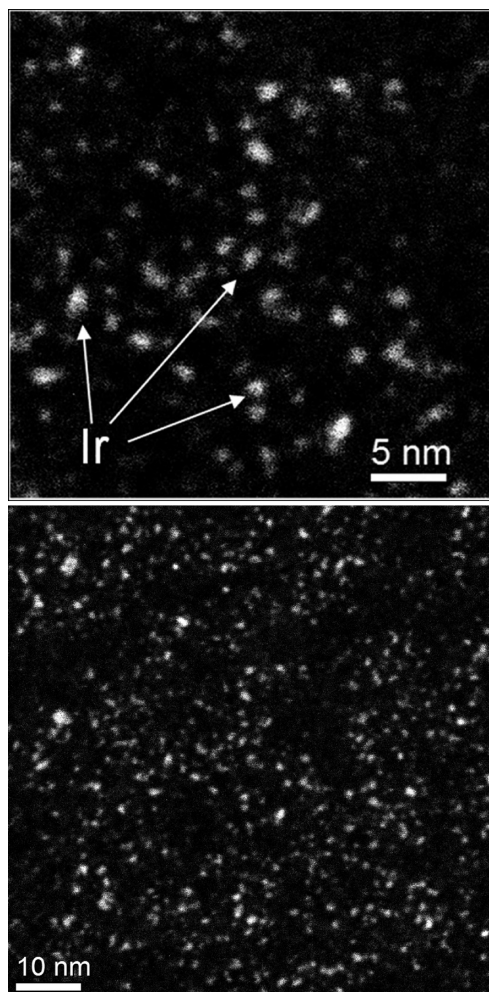
Figure 7. Example Z-contrast images of the [(1,5-COD)Ir(μ-O$_2$C$_8$H$_{15}$)]$_2$ plus AlEt$_3$, Al/Ir = 2.0, catalyst sample *after hydrogenation*. The Ir cluster histogram from the diameter measurement of 635 Ir clusters is also shown. The mean Ir cluster diameter is 1.0 ± 0.3 nm, which corresponds to Ir(0)$_{\sim40}$ clusters. Two larger Ir nanoclusters with diameters of 3.1 and 3.8 nm are also observed, presumably the result of well-precedented nanocluster aggregation processes.[64,65]

with Al/Ir ratios of 1.0, 2.0, and 5.0.[66] An example HRTEM image of the sample with an Al/Ir ratio of 2.0, Figure 8, shows distinct lattice fringes in the Ir particles. This result is general to all Al/Ir ratios tested; crystalline Ir Ziegler

(60) Whetten, R. L.; Khoury, J. T.; Alvarez, M. M.; Murthy, S.; Vezmar, I.; Wang, Z. L.; Stephens, P. W.; Cleveland, C. L.; Luedtke, W. D.; Landman, U. *Adv. Mater.* **1996**, *8*, 428–433.

(61) Khitrov, G. A.; Strouse, G. F. *J. Am. Chem. Soc.* **2003**, *125*, 10465–10469.

(62) Kuzuya, T.; Tai, Y.; Yamamuro, S.; Sumiyama, K. *Chem. Phys. Lett.* **2005**, *407*, 460–463.

(63) Maya, L.; Chen, C. H.; Stevenson, K. A.; Kenik, E. A.; Allman, S. L.; Thundat, T. G. *J. Nanoparticle Res.* **2002**, *4*, 417–422.

(64) Hornstein, B. J.; Finke, R. G. *Chem. Mater.* **2004**, *16*, 139–150.

(65) (a) Besson, C.; Finney, E. E.; Finke, R. G. *J. Am. Chem. Soc.* **2005**, *127*, 8179–8184. (b) Finney, E. E.; Finke, R. G. *Chem. Mater.* **2008**, *20*, 1956–1970.

(66) Images of catalyst samples *after* their use in hydrogenation were also obtained using bright field TEM. The images can be found in the Supporting Information.
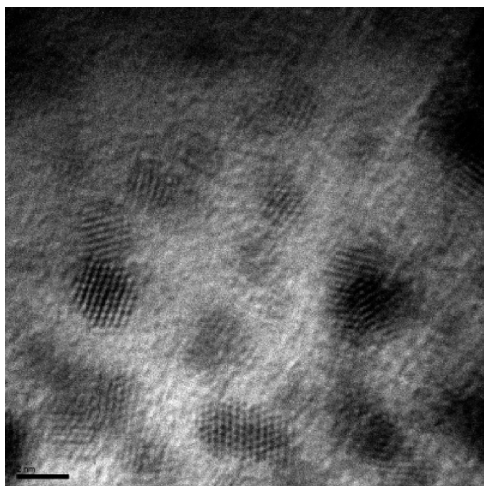
Figure 8. An example HRTEM image of the [(1,5-COD)Ir(μ-O$_2$C$_8$-H$_{15}$)]$_2$ plus AlEt$_3$ catalyst, Al/Ir is 2.0, after its use in cyclohexene hydrogenation (scale bar is 2 nm). The distinct lattice fringes show that the Ir particles after use in hydrogenation possess a crystalline structure under the HRTEM observation conditions. Crystalline particles are observed for all Al/Ir values tested, 1.0, 2.0, and 5.0.

nanoclusters are observed in all HRTEM images obtained for the samples with Al/Ir ratios of 1.0, 2.0, and 5.0 (other images are shown in Figures S27−S30, Supporting Information). Electron diffraction shows that these Ziegler nanoclusters after hydrogenation are *fcc* Ir, at least under the conditions of the electron beam (Figure S31, Supporting Information). The key result, then, of the combined Z-contrast and HRTEM microscopy is that the mean Ir$_n$ clusters postcatalysis are larger, crystalline 1.0 ± 0.3 nm, Ir$_{\sim40}$ nanoclusters.

Identification of the Ir-Containing Species in the AlEt$_3$/Ir Catalyst *after* Hydrogenation: XAFS Spectroscopy. A sample of the [(1,5-COD)Ir(μ-O$_2$C$_8$H$_{15}$)]$_2$ plus AlEt$_3$ catalyst, with an Al/Ir ratio of 1.0, after its use in cyclohexene hydrogenation was analyzed by XAFS spectroscopy. Peaks in the 3−6 Å range of the FT magnitude spectrum reveal that the sample is composed of Ir$_n$ particles with ordered internal atomic structures, Figure 9, consistent with the microscopy results (vide supra). A fit of the Fourier transform magnitude spectrum, also shown in Figure 9, gives an Ir−Ir 1NN coordination of 9.0 ± 0.4. The mean coordination number, obtained from fitting the Ir−Ir 1NN contribution, was used to estimate cluster sizes using a theoretical mean coordination number−particle diameter correlation curve[16,27,67] (Supporting Information). An Ir−Ir 1NN coordination of 9.0 ± 0.4 according to XAFS corresponds to, on average, 1.6 nm, crystalline *fcc* Ir(0)$_{\sim150}$ clusters. Additionally, the Ir−Ir 1NN distance of 2.688 ± 0.001 Å is now *shorter* than that in bulk Ir, as one would expect for nanometer-sized, contracted surface[31,39] clusters. Full fitting results are given in Table S8, Supporting Information.

The XANES portion of the sample spectrum is essentially identical to the XANES spectra of Ir black, Figure 10. This shows convincingly that the oxidation state of the Ir in the sample is Ir(0). XPS confirms the predominance of Ir(0) in a catalyst sample with an Al/Ir ratio of 2.0, after hydrogenation. Additionally, the XANES result, especially with

(67) Montejano-Carrizales, J. M.; Morán López, J. L. *Nanostruct. Mater.* **1992**, *1*, 397–409.
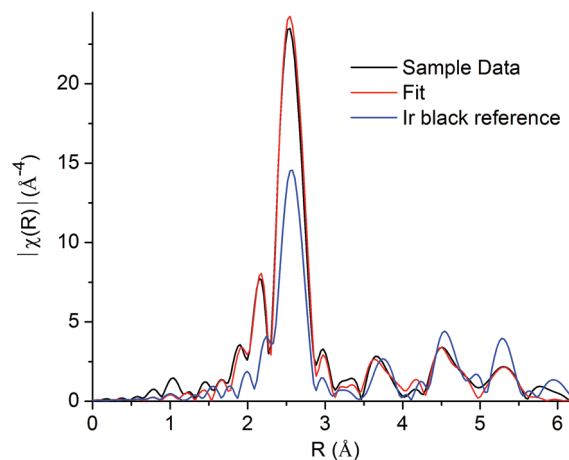
Figure 9. Fourier transform (FT) magnitudes of the data (black curve) and fit (red) of a powder sample of the Al/Ir = 1.0 catalyst after its use in hydrogenation. The longer range scattering peaks in the 3−6 Å range are expected for Ir nanoclusters with ordered internal structures. The Ir−Ir 1NN coordination number obtained from the fit, 9.0 ± 0.4, corresponds to, on average, approximately 1.6 nm, crystalline *fcc* Ir(0)$_{\sim150}$ clusters, according to XAFS. The FT magnitude spectrum of the Ir black reference, scaled by one-fourth, is shown for comparison (blue).
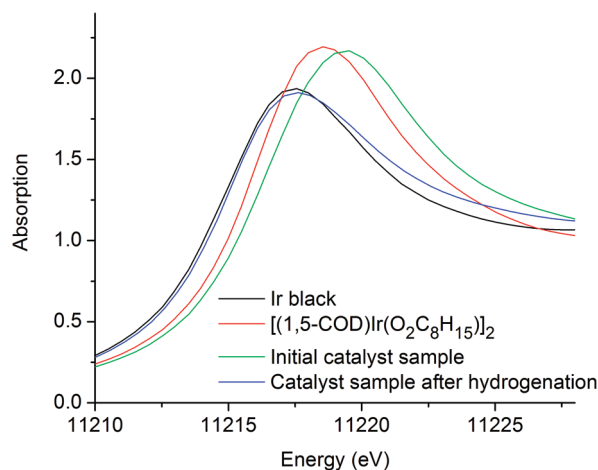

Figure 10. XANES spectra of Ir black (black line), the precatalyst [(1,5-COD)Ir(μ-O$_2$C$_8$H$_{15}$)]$_2$ (red), the initial [(1,5-COD)Ir(μ-O$_2$C$_8$H$_{15}$)]$_2$ plus AlEt$_3$ catalyst (green), and the same catalyst sample after its use in the catalytic hydrogenation of cyclohexene (blue). The similarity of the Ir black and after-hydrogenation catalyst curves is compelling evidence for an Ir(0) oxidation state in the after-hydrogenation catalyst.

corroboration by XPS independently performed on a different sample (Supporting Information), shows definitively that the sample analyzed by XANES and XAFS was not contaminated by atmospheric oxygen. In short, the XAFS plus XANES and XPS of post hydrogenation catalyst samples shows the presence of, on avergage, approximately 1.6 nm, *fcc* Ir(0)$_{\sim150}$, nanoparticles.

The difference in mean Ir cluster sizes measured by Z-contrast STEM versus those approximated by XAFS spectroscopy for the after-hydrogenation samples is possibly due to the XAFS data being collected on a powder sample. In a control experiment, precipitated catalyst material was collected after an initial cyclohexene hydrogenation run and isolated as a powder. It was then redispersed in cyclohexane, cyclohexene was added, and run in a second hydrogenation (see the Experimental Section for more details). Catalytic cyclohexene hydrogenation begins immediately using
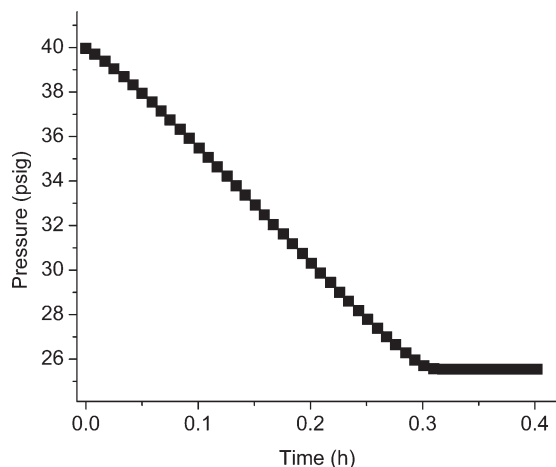
Figure 11. A second cyclohexene catalytic run following collection and isolation of a precipitate from a first run, and redispersion of it in cyclohexane. The initial hydrogenation rate in this experiment is 47 psig/h, and the maximum rate is 50 psig/h. Both rates are similar to the maximum hydrogenation rate observed from aged catalyst solutions during an initial run.

redispersed precipitate for a second run, Figure 11, and at a similar rate to the maximum rate achieved toward the end of an initial run, Figure 1. In short, this control experiment confirms that a highly active hydrogenation catalyst is retained following the procedures used to analyze the catalyst sample by XAFS and XANES. Add to this the observation, mentioned previously, that catalyst solutions sometimes precipitate after a cyclohexene hydrogenation run under standard conditions, and the combined results argue strongly that the postcatalysis Ir cluster characterization results from XAFS are representative of the nature of the Ir species postcatalysis (although analysis of the precipitate, likely the result of well-precedented nanocluster aggregation processes,[64,65] probably gives a larger Ir particle size than what exists in solution before precipitation occurs). The key point is that *fcc* $Ir(0)_n$ Ziegler nanoclusters are increasing in size and abundance postcatalysis. Moreover, they likely are the fastest, best catalysts in this system (on the basis of the results of this control experiment, the increase in the rate of cyclohexene hydrogenation as catalysis proceeds, Figure 1, and based on catalyst poisoning studies, vide infra).

Identification of the Ir-Containing Species in the $AlEt_3$/Ir catalyst *after* hydrogenation: MALDI MS. The $[(1,5-COD)Ir(\mu-O_2C_8H_{15})]_2$ plus $AlEt_3$, Al/Ir = 2.0, catalyst, after its use in cyclohexene hydrogenation, was analyzed using MALDI MS (the spectrum is shown in the Supporting Information). Similar to the MALDI MS results from the sample analyzed before hydrogenation, a broad peak representing a range of Ir_n species exists in the ≥ 1000 m/z region, with a maximum at about 3000 m/z corresponding to $Ir_{\sim 16}$, approximately 0.8-nm-diameter clusters. However, this posthydrogenation peak has a significant shoulder at about 5500 m/z, which indicates $Ir_{\sim 30}$, 0.9 nm clusters, and the FWHM of the peak corresponds to $Ir_{\sim 8-40}$, 0.6−1.0-nm-diameter clusters (the FWHM was used to estimate mean cluster diameter, Table 1, although it is an underestimation even more so than with the prehydrogenation sample because of the irregular peak shape). In addition, the curve tails off toward higher m/z values considerably less steeply than in the prehydrogenation sample spectrum—it reaches

one-quarter max intensity at about 11500 m/z, which corresponds to $Ir_{\sim 60}$, 1.2 nm clusters (nearly double the ~ 6000 m/z at one-quarter intensity in the prehydrogenation spectrum, vide supra), and falls to one-eighth the maximum intensity at $\sim 19\,500$ m/z, which corresponds to $Ir_{\sim 100}$, 1.4 nm clusters (again, about double the m/z value at one-eighth maximum intensity in the prehydrogenation sample that corresponds to $Ir_{\sim 50}$, 1.1 nm clusters).

A broad range of Ir_n cluster sizes is again observed using MALDI MS, but compared to the prehydrogenation sample, the posthydrogenation catalyst includes even larger Ir_n nanoclusters, and a significantly greater quantity of these larger Ir_n species. Again, MALDI MS gives results that are similar, but not identical, to those from Z-contrast STEM; the possible reasons may be any combination of the factors listed previously, and an additional factor may be the difference in transit time between completion of a catalytic run and analysis of the sample.[68] The key point that remains, regardless of the differences in Ir_n cluster sizes obtained using the three methods, is that Z-contrast STEM, XAFS, and MALDI MS *all show a distinct trend toward a greater population of larger, nanoscale Ir_n clusters in the posthydrogenation catalyst sample*. On the basis of the combined results of these three methods (Z-contrast giving mean 1.0 ± 0.3 nm, $Ir_{\sim 40}$ clusters; XAFS indicating mean 1.6 nm, $Ir_{\sim 150}$, clusters; and MALDI MS also showing a shift in the population if Ir_n species toward larger, nanometer scale clusters) we refer to these nanoscale, crystalline $Ir(0)_n$ clusters herein as *fcc* $Ir(0)_{40-150}$ Ziegler nanoclusters.

The Before-Hydrogenation-to-After-Hydrogenation Changes of Aged Catalysts: A Summary. The first step in the approach used herein to address the "is it homogeneous or heterogeneous catalyst?" question for the present catalyst system,[3,4b,7,8] is identification of the form(s) (e.g., Ir_n cluster nuclearity) that the observable catalyst mass takes. A combination of analytic techniques has revealed that catalyst solutions before their use in hydrogenation contain a broadly dispersed range of Ir_n clusters extending from mono-Ir compounds to Ir_n nanoclusters with significantly disordered internal atomic structures, and with an estimated average of 0.5−0.7 nm, $Ir(0)_{\sim 4-15}$ clusters. *The Ir_n species present are nearly the same regardless of the Al/Ir ratio employed*, an important finding in its own right which, in turn, suggests *that the observed changes in catalytic activity at different Al/Ir ratios are primarily the result of changes in the form and function of the Al-derived component(s) of the catalyst* (i.e., the Al/Ir ratio not causing significant changes in the Ir_n nuclearity).[13] During the use of these solutions in hydrogenation, a conversion toward roughly 1.0−1.6 nm,

---

(68) MALDI MS experiments were performed directly after the end of catalytic runs, whereas Z-contrast STEM (and XAFS spectroscopy) required ≥2 days between the end of the catalytic run and analysis (primarily for transit). This difference in procedures could affect the particle sizes measured, which makes some sense; catalyst samples sometimes precipitate a dark brown powder after the end of a catalytic run under standard conditions anyway. The observation of a precipitate suggests that Ir_n cluster agglomeration or growth processes initiated during catalysis continue post-catalysis. Ultimately, these observations argue against the reliability of precise, *specific* Ir_n cluster sizes as measured by Z-contrast STEM, MALDI MS, and XAFS spectroscopy, but strongly argue *for* the development of *fcc* $Ir(0)_n$ Ziegler nanoclusters in this system in general.

fcc Ir(0)$_{\sim40-150}$ Ziegler nanoclusters takes place,[69] consistent with the color change of the catalyst solutions from tawny yellow to darker brown as hydrogenation proceeds and the precipitation often seen a few days after the conclusion of a catalytic run. The conversion toward these 1.0–1.6 nm, Ir(0)$_{\sim40-150}$ Ziegler nanoclusters is independently evidenced by the results of Z-contrast STEM, XAFS spectroscopy, and MALDI MS, which show shifts in the range of Ir$_n$ clusters present toward larger Ir$_n$ clusters and increases in the mean observed clusters sizes and mean Ir$_n$ nuclearities. A key to obtaining these insights is our use of a third-row Ir system where, the evidence argues, its more stable Ir–Ir bonds mitigate against artifacts due, for example, to sample preparation and ex situ Z-contrast STEM.

Additional Kinetics-Based Experiments Probing the Active Catalyst. Kinetics data are key to determining whether the observed catalytic activity using [(1,5-COD)Ir(μ-O$_2$C$_8$H$_{15}$)]$_2$ plus AlEt$_3$ catalysts is homogeneous (e.g., defined here as proceeding via mono-Ir compounds or subnanometer Ir$_{\sim4-15}$ cluster catalysts) or heterogeneous (e.g., defined here as proceeding via Ir(0)$_{\sim40-150}$ Ziegler nanoclusters).[3,4b,7,8] We have already shown that catalytic cyclohexene hydrogenation curves obtained using the [(1,5-COD)Ir-(μ-O$_2$C$_8$H$_{15}$)]$_2$ plus AlEt$_3$ catalyst with an Al/Ir ratio of 2, both with and without prior aging of the catalyst solutions for 9 h, give a maximum hydrogenation rate (−d[H$_2$]/dt) that is *not* the initial rate (i.e., that is faster than the initial rate). Instead, the hydrogenation rate increases concomitant with the increase in cluster size (and corresponding structural change) from Ir$_{\sim4-15}$ to *fcc* Ir(0)$_{\sim40-150}$. This rate increase is quite pronounced when using catalyst solutions immediately after their preparation (see the switch in activity at $\sim$2 h in Figure 12b) but is more modest when the catalyst solutions have been aged, Figure 12a. The observed increase in the rate of hydrogenation during catalysis, plus the above studies showing (i) the *presence* of larger Ir(0)$_{\sim40-150}$ Ziegler nanoclusters post catalysis and also (ii) *high catalytic activity* when these nanoparticles are collected as a precipitate, redispersed in cyclohexane and used for a second catalytic run, strongly suggests, in the simplest (Ockham's razor) interpretation of the data, *that the fastest, best catalysts are the larger fcc* Ir(0)$_{\sim40-150}$ *Ziegler nanoclusters.*

To further test this hypothesis that the larger *fcc* Ir(0)$_{\sim40-150}$ Ziegler nanoclusters are the kinetically dominant catalyst, Hg(0) poisoning experiments were utilized (Hg(0) being known to poison most heterogeneous catalysts[3,4b,70−72]). Specifically, Hg(0) was added
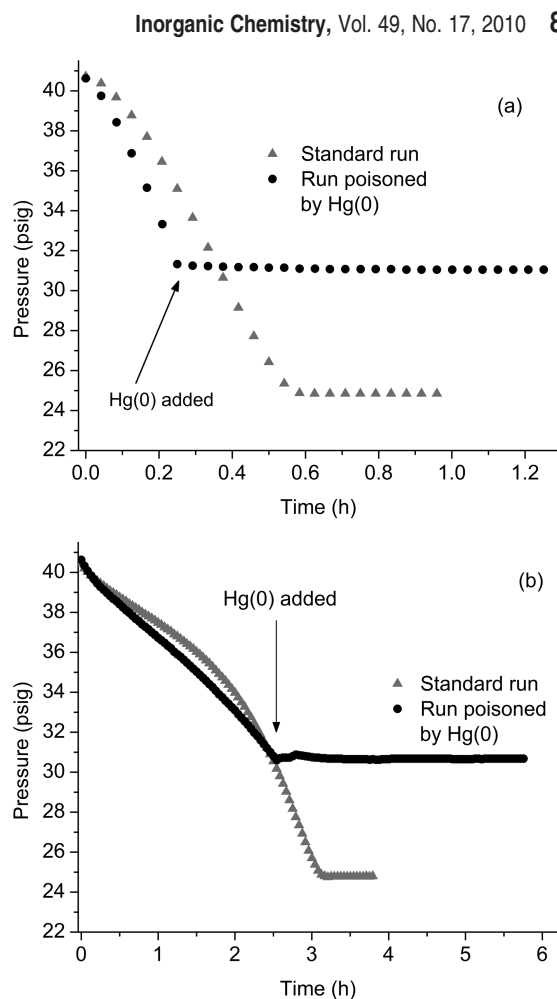
Figure 12. Cyclohexene hydrogenation curves for [(1,5-COD)Ir(μ-O$_2$C$_8$H$_{15}$)]$_2$ plus AlEt$_3$ catalysts with Al/Ir ratios of 2.0, for (a) catalyst solutions aged 9 h or (b) not aged, alongside hydrogenation runs poisoned by the addition of Hg(0) under otherwise identical conditions. The variation in the hydrogenation runs prior to Hg(0) addition is typical for this system. For runs poisoned by Hg(0), the catalytic hydrogenation of cyclohexene was allowed to proceed until the maximum rate regime was reached. Then, the solution was transferred to the drybox where ≥300 equivalents of Hg(0) per Ir was added and allowed to stir at 1000 rpm before putting it back on the hydrogenation line. The *subsequent* part of the hydrogenation curve shows *immediate and total* poisoning of the catalyst.

to the catalyst solutions after the cyclohexene consumption had proceeded about halfway (i.e., and once the catalytic rate had entered the maximum activity regime). The catalysis was poisoned *immediately and completely* by the Hg(0) addition, regardless of whether the initial catalyst solution was aged for 9 h prior to use (Figure 12a) or used immediately without aging (Figure 12b). This result provides additional evidence that the catalyst at the most active stage is what we defined earlier as heterogeneous—that is, due to the *fcc* Ir(0)$_{\sim40-150}$ Ziegler nanoclusters observed post hydrogenation.

As a control experiment, Hg(0) was added to catalyst solutions, both with and without aging, *before* the start of catalytic cyclohexene hydrogenation (i.e., before being exposed to H$_2$ gas). Near-immediate poisoning of the catalyst, Figure 13, suggests that the kinetically competent, fastest catalysts, even at the initial stage, are heterogeneous (i.e., larger Ir$_n$ nanoclusters, *not* the initially present mono-Ir complexes and Ir$_{\sim4-15}$ clusters, although one cannot rule out that Hg(0) is poisoning active Ir$_{\sim4-15}$ subnanoclusters).

(69) The details of this structural transformation are currently unknown in this system, although for a report of a similar phenomenon in rhodium particles upon exposure to H$_2$, see: Choukroun, R.; De Caro, D.; Chaudret, B.; Lecante, P.; Snoeck, E. *New J. Chem.* **2001**, *25*, 525−527.

(70) Phan, N. T. S.; Van Der Sluys, M.; Jones, C. W. *Adv. Synth. Catal.* **2006**, *348*, 609−679.

(71) Weddle, K. S.; Aiken, J. D.; Finke, R. G. *J. Am. Chem. Soc.* **1998**, *120*, 5653−5666.

(72) Catalyst poisoning by Hg(0) is, by itself, an imperfect test for homogeneity or heterogeneity, as has been pointed out previously.[4b,70] However, it can be useful, especially considering the challenges posed by identifying Ziegler-type hydrogenation catalysts.[3] One concern with the Hg(0) catalyst poisoning test is that, due to the insolubility of Hg(0), it may be difficult to thoroughly contact/react the Hg(0) with all of the catalyst in solution.[4b] This concern is addressed herein by using > 300 equivalents of Hg(0) per Ir each time, and by a series of control experiments showing the 24 h of mixing time allowed was necessary and sufficient for poisoning of these particular catalysts. That effective procedure was followed for each subsequent Hg(0) poisoning experiment.
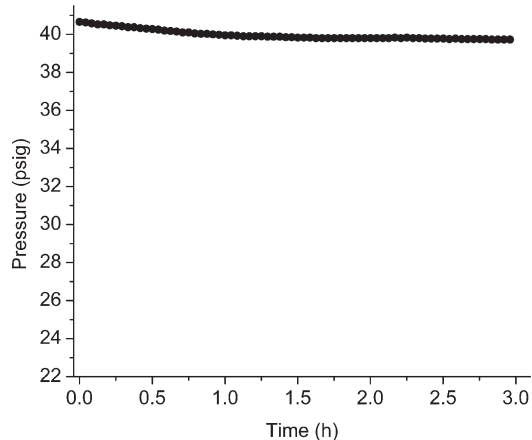
Figure 13. Near-immediate poisoning of the catalyst. Hg(0), ≥ 300 equivalents per Ir, was added to the catalyst solution after its preparation and 9 h of aging in the drybox. Sufficient mixing was ensured by stirring of the Hg(0)-containing catalyst solution for 24 h at 1000 rpm. Poisoning is 95% complete, but a small, residual, ca. 5% activity (i.e., 5% of the H_2) is still consumed, mostly early in the experiment.

However, and interestingly, although ~95% of the activity is poisoned, there is ~5% activity initially, non-Hg(0)-poisoned activity that implies a residual, *apparently* homogeneous catalyst, albeit one that accounts for only ~5% of the catalysis.[73] Whether Hg(0) will or will not poison subnanometer, molecular Ir_n clusters remains an open question, one that will require the synthesis and characterization of, for example, authentic Ir_4 clusters and attempts to poison their expected catalysis with Hg(0). If, for example, the present prehydrogenation Ir clusters are actually of nominal composition $Ir(I)_4H_4$ (i.e., $Ir(I)_4$ and not $Ir(0)_4$), then that would be one *possible* explanation for their insensitivity to Hg(0). Nevertheless, the Hg(0) poisoning experiments provide additional support for the hypothesis—now the dominant hypothesis for further studies in the area of Ziegler-type hydrogenation catalysis—that th*e most active, kinetically competent catalysts* at the point of the maximum hydrogenation rate are *heterogeneous Ziegler nanoclusters analogous to the present $Ir(0)_{\sim 40-150}$*. This is an important, previously unavailable finding. It presages an area of catalysis by hydrocarbon-soluble, Lewis-acid-containing, and thus presumably unusually coordinatively unsaturated—and certainly extremely catalytically active, industrially utilized—"Ziegler nanocluster" catalysts.

Summary

The main findings of this study, then, are as follows:
- The initial $[(1,5\text{-COD})Ir(\mu\text{-}O_2C_8H_{15})]_2$ plus $AlEt_3$ Ziegler-type hydrogenation catalyst solutions, *before* hydrogenation, are (by Z-contrast STEM, XAFS, and MALDI MS) a broad range of Ir_n

(73) Two of the three trials using catalysts without aging gave poisoning results similar to that in Figure 13 (i.e., nearly complete poisoning after an initial small H_2 pressure loss). Interestingly, however, even with the ≥ 300 equivalents of Hg(0) per Ir used and an identical procedure used in each case, in one of the three trials, the Hg(0) only disturbed the shape of the hydrogenation curve but failed to prevent substrate hydrogenation. The implication is that an initial homogeneous Ir catalyst has at least some resistance to reaction with, or poisoning by, Hg(0) (although, Hg(0) is also believed to be able to poison homogeneous catalysts in some cases[70]). These other Hg(0) poisoning control experiments are shown in the Supporting Information for the interested reader.

complexes from mono-Ir compounds to noncrystalline Ir_n Ziegler nanoclusters, with the estimated mean Ir_n clusters being 0.5–0.7 nm, $Ir_{\sim 4-15}$ subnanometer clusters. The agreement among the results, regardless of whether ex situ solid state Z-contrast imaging or in situ, solution XAFS/XANES is employed, argues against artifacts caused by these methods or the associated sample handling or preparation. Our use of MALDI MS as an additional method yielded estimated mean Ir cluster size and nuclearity results that are similar to those obtained by Z-contrast STEM and XAFS, but not identical—results that we view as a calibration of the less useful MALDI-MS method in the present case. Nevertheless, the results all yield a consistent picture of the catalyst before hydrogenation as consisting of a broad range of Ir_n species dominated by subnanometer Ir_n clusters.

- According to XAFS, the Ir_n nuclearity results are largely unchanged regardless of the Al/Ir ratio employed. This important observation indicates that differences in catalytic activity, as a function of Al/Ir ratios, must be due just to the form or function of the Al-derived component(s),[13] and not to any Al/Ir-controlled or -dependent nuclearity of the initial Ir_n species present.

- At the end of their use in hydrogenation, the population of Ir_n clusters in the samples has shifted toward larger, 1.0–1.6 nm, *fcc* $Ir(0)_{\sim 40-150}$ Ziegler nanoclusters. The average sizes of these larger nanoclusters, as determined by Z-contrast STEM, HRTEM, and XAFS/XANES, are similar, but not identical, depending on the technique (and associated sample preparation) used. However, the *trend* toward larger, $Ir(0)_{\sim 40-150}$ Ziegler nanoclusters in posthydrogenation samples is verified by each method (i.e., is method-independent).

- Significantly, the development of *fcc* $Ir(0)_{\sim 40-150}$ nanoclusters correlates with both a change in solution color (that also signals nanocluster formation) and an increase in the rate of cyclohexene hydrogenation. Furthermore, a precipitate can be collected from the catalyst solutions and, when redispersed in cyclohexene, displays immediate high activity for the hydrogenation of cyclohexene comparable to the maximum activity observed toward the end of an initial cyclohexene hydrogenation run. The evidence is consistent with and highly supportive of the now-dominant hypothesis for future research in the area, that the larger *fcc* $Ir(0)_{\sim 40-150}$ Ziegler nanoclusters are the fastest Ziegler-type hydrogenation catalysts attained in at least the present Ir Ziegler-type catalyst system. That said, catalysis of a ~2- to 10-fold slower rate (depending on the Al/Ir ratio and whether an aged or nonaged catalyst was used) is seen initially, when the estimated mean Ir species present are 0.5–0.7 nm, $Ir_{\sim 4-15}$ clusters.

- Consistent with the above "Ziegler nanocluster catalysis hypothesis", Hg(0) added to catalyst solutions after the catalysts have entered their maximum rate regime stops the catalytic activity

immediately and completely. This further supports evidence that the fastest catalysts found in this system are the *fcc* Ir(0)$_{\sim 40-150}$ Ziegler nanoclusters (i.e., that "heterogeneous catalysis"[3,4] is present). However, it is worth noting that in solutions with Hg(0) added at the prehydrogenation stage, residual catalysis, presumably effected by unpoisoned homogeneous catalyst(s) such as monometallic Ir complexes or 0.5−0.7 nm, Ir$_{\sim 4-15}$ clusters, results in ∼5% of the normal total H$_2$ consumption. Although significant catalysis by discrete subnanometer Ir species is not unequivocally ruled out by this study, the overall simplest interpretation of the data is that the larger, *fcc* Ir(0)$_{\sim 40-150}$ nanoclusters are the more effective catalysts.

- Successfully investigating the problem of the composition and structure of a Ziegler-type hydrogenation catalyst has depended on the approach used herein: (a) the use of a third-row Ir-system with its strong Ir−Ir bonds and, therefore, more robust Ir$_n$ species that are less sensitive to various analytical methods and associated sample preparations, (b) the development[2] and use of the well characterized [(1,5-COD)Ir(μ-O$_2$C$_8$H$_{15}$)]$_2$ precatalyst, and (c) the use of a combination of multiple, complementary analytical techniques *and* kinetic studies plus poisoning studies. That said, additional, ideally operando studies are desirable in this area,[3,9] and it is now possible to design them rationally and effectively.

- To our knowledge, this is the first report for a Ziegler-type hydrogenation catalyst where identification of the Ir$_n$ species present using multiple complementary techniques has been coupled to kinetic evidence to show that the best, fastest catalysts are, in all probability,[20,74,75] the larger, *fcc* Ir(0)$_{\sim 40-200}$ Ziegler nanoclusters. Nor has evidence

been previously reported that a Ziegler-type hydrogenation catalyst can initially contain a homogeneous component (ca. 5% of the activity) and transition to heterogeneous catalysis during hydrogenation. That said, we wish to emphasize once again (vide supra; the Introduction) the important, recent contributions of, especially, Shmidt[5] and co-workers and Bönnemann and co-workers[3,6] that also provide evidence for the presence of nanoclusters under Ziegler-type hydrogenation catalysis conditions.

- Further investigation of this prototype Ir Ziegler-type hydrogenation system through additional kinetic studies,[12] and evidence for the forms and roles of the AlR$_3$-derived component of the catalyst, will be reported elsewhere.[13] Those studies include an interesting inverse relationship between the maximum TOF and [Ir] concentration, intriguing findings which have required their own, separate study.[12] In addition, the results of studies analogous to those herein using the Co and Ni systems commonly employed by industry for olefin and polymer hydrogenation will be reported in due course.[14]

Our comprehensive review of the literature of Ziegler-type hydrogenation catalysts[3] shows the above insights (i.e., into the products of the precatalyst and cocatalyst reaction, how those products develop with use in a hydrogenation reaction, and the relative activities of those (metal)$_n$ products) are at the state-of-the-art for a Ziegler-type hydrogenation catalyst—despite the industrial use of Ziegler-type hydrogenation catalysts for ∼50 years to hydrogenate, currently, around 1.7×10^5 metric tons of styrenic block copolymers annually.[2] One of our hopes is that the present demonstration, that at least Ir$_n$ "Ziegler-type nanoclusters" both exist and are also the kinetically dominant, highly active catalysts, will prompt the community to begin to make use of these and other highly coordinately unsaturated, relatively "weakly ligated/labile ligand",[76] hydrocarbon-soluble nanoclusters. Such Ziegler-type nanoclusters are unusual in that RCO$_2^-$ from the starting material, *hydrocarbon* solvent, and Lewis acidic AlEt$_3$ (plus their expected adducts, e.g., RCO$_2$AlEt$_3^-$ and any Al−O−Al containing alumoxane from trace H$_2$O) are the only possible (weakly ligating) ligands present, undoubtedly one reason for the high, industrial-level catalytic activity of Ziegler nanoclusters.

Experimental Section

Materials. Unless stated otherwise, all materials were handled and stored under N$_2$ in a Vacuum Atmospheres drybox, with O$_2$ levels continuously maintained at ≤5 ppm according to a Vacuum Atmospheres O$_2$-level monitor. All solution measurements and additions done in the drybox at Colorado State University (CSU) utilized gastight syringes. Glassware was dried in an oven at 160 °C for ≥12 h and cooled under a vacuum or dry N$_2$. Cyclohexane (Sigma-Aldrich, 99.5%, H$_2$O < 0.001%) was kept over activated molecular sieves for ≥2 days prior to use. Molecular sieves (Acros, 3 Å) were activated by heating at 200 °C for 6 h under a vacuum. The precatalyst [(1,5-COD)Ir(μ-O$_2$C$_8$H$_{15}$)]$_2$ was prepared as described[2] and used herein as a solution in cyclohexane, typically 9.0 or 12.0 mM in [Ir]. AlEt$_3$ (Strem Chemicals, 93%) was also used as a cyclohexane solution, typically 18.0 or 36.0 mM.

(74) Liang, A. J.; Gates, B. C. *J. Phys. Chem. C* **2008**, *112*, 18039–18049.

(75) (a) One, of course, never *proves* anything in science, including the form of the catalyst. Bergman's formulation of "Halpern's Guidelines or Rules for Catalysis" apply here—that the observable species are many times not the catalyst.[20] That said, nonpoisoned nanoclusters are a somewhat different case, at least according to all of our knowledge of metal particle catalysis. Restated, any Ir(0)$_n$ nanocluster that is not poisoned by basic ligands is expected to be a (good hydrogenation) catalyst. This is especially true in the present case, the current Ir/AlEt$_3$ Lewis acid/cyclohexane catalyst system, where the best (∼only) ligands are the cyclohexene and H$_2$ reactants (i.e., AlEt$_3$ and cyclohexane being poor "Lewis *bases*"). Hence, the dominant observable form(s) and sizes of the nanoclusters are expected—and assumed herein if you like—to correlate closely with the dominant catalyst for the present *structure insensitive* hydrogenation reactions. One alternative possibility is that the active catalysts are the result of fragmentation of the observed clusters under catalytic conditions. For example, Gates and co-workers have shown that the nuclearity of *oxide-supported* Rh$_n$ and Ir$_n$ species can be reversibly altered on the basis of the composition of an ethylene−H$_2$ gas mixture to which they are exposed;[58d,74] small M$_{2-4}$ cluster species oxidatively fragment to M$_1$ under ethylene (i.e., catalytic conditions with substrate present) but can reform under H$_2$. However, the conditions of those studies (oxide-supported catalysts, gas phase substrate, no solvent) are very different than those employed herein. Another, perhaps more relevant example is the current debate concerning the true catalyst species in Pd-catalyzed coupling reactions such as Suzuki coupling and Heck arylation. There is disagreement as to whether catalysis is affected by the Pd nanoparticles themselves, or by molecular Pd species that fragment from the larger, inactive clusters.[70] In the final analysis, the result of the present study is to present Ir(0)$_{\sim 40-150}$ Ziegler-type nanocluster hydrogenation catalysts as the leading hypothesis for future studies of the true catalyst.

(76) For lead references, see the following and references therein: (a) Mondloch, J. E.; Wang, Qi; Frenkel, A. I.; Finke, R. G. *J. Am. Chem. Soc.* **2010**, *132*, 9701−9714. (b) Bayram, E.; Zahmakiran, M.; Özkar, S.; Finke, R. G. *Langmuir* **2010**, *26*, 12455−12464.

Caution! Alkylaluminums are pyrophoric and should be handled with care using air- and moisture-free techniques.[77]

Cyclohexene (Aldrich, 99%) was distilled over sodium under argon. Both Ar and H_2 gases were passed through moisture (Scott Specialty Gases) and oxygen traps (Trigon Technologies) prior to use. Ir black and $Ir_4(CO)_{12}$ (Strem, 98%) were used as received. HPO_4-stabilized *fcc* $Ir(0)_n$ nanos were synthesized as previously described (details are provided in the Supporting Information).[26]

Catalyst Solution Preparation. Catalyst solutions were prepared in the drybox at CSU both in batches and in smaller volumes for individual hydrogenation use (the temperature in the drybox was between 25 and 30 °C). For example, a 20 mL, [Ir] = 1.44 mM, batch of catalyst with an Al/Ir ratio of 2 was prepared by first adding 15.2 mL of cyclohexane to a 20 mL glass vial containing a $5/8 \times 5/16$ in. Teflon-coated magnetic stir bar. Next, 2.4 mL of a cyclohexane solution of $[(1,5-COD)Ir(\mu-O_2C_8H_{15})]_2$, 12.0 mM in [Ir], was added, making an orange/light red solution. Stirring (1000 ± 200 rpm, measured with a Monarch Instruments Pocket-Tachometer 100) was started, and 1.6 mL of a 36.0 mM $AlEt_3$ solution was added rapidly.

Catalytic Cyclohexene Hydrogenations. All catalyst solutions for cyclohexene hydrogenation were prepared individually in 22×175 mm Pyrex culture tubes containing a new $5/8 \times 5/16$ in. Teflon-coated magnetic stir bar (both rinsed three times with ultrapure water prior to drying). For example, a 0.6 mM in [Ir], Al/Ir = 2.0, catalyst solution was prepared by adding 0.20 ± 0.01 mL of a 9.0 mM in [Ir] cyclohexane solution of $[(1,5-COD)Ir(\mu-O_2C_8H_{15})]_2$ to a culture tube followed by 0.200 ± 0.002 mL of 18.0 mM $AlEt_3$ in cyclohexane, added rapidly with 1000 ± 200 rpm stirring to make Al/Ir = 2.0. Cyclohexane was added to bring the total volume to 2.5 mL, and then 0.5 ± 0.01 mL of cyclohexene was added, making 3.0 mL of a Al/Ir = 2 catalyst solution, 0.6 mM in [Ir] and 1.65 M in [cyclohexene].

The procedure and apparatus used for catalytic hydrogenations of cyclohexene were described in detail elsewhere.[7a,78,79] Briefly, once the hydrogenation reaction solution was prepared, the culture tube was placed in a Fisher–Porter (F–P) bottle, which was then sealed. The solution was then allowed to stir at 1000 rpm in the sealed F–P bottle in the drybox, typically for 9 h (see Figure S2, Supporting Information). At the end of the aging period, if any, the F–P bottle was then brought out of the drybox and placed in a bath set at 22.0 ± 0.1 °C. Stirring was started at 1000 ± 10 rpm employing a Fauske Super Magnetic Stirrer, and the F–P bottle was connected to a pressurized H_2 line using Swagelock quick-connects. The F–P bottle was purged 15 times (1 purge/15 s). The pressure in the F–P bottle was set to 40 psig, and data collection was initiated at 4 min after the first purge. Hydrogen pressure vs time data were collected using a pressure transducer (Omega PX 624–100 GSV) interfaced via an Omega D1131 analog-to-digital converter connected to a PC running LabView 7.0. Data were subsequently handled using MS Excel and Origin 7. In order to quantitatively compare hydrogenation rates, and because of their shapes (i.e., more rapid H_2 pressure loss later in the hydrogenation, as opposed to initially), the initial and maximum rate portions of the curves were fit separately by polynomial and linear expressions, respectively (for an example, see Figure S1 of the Supporting Information).

Catalyst Poisoning by Hg(0). All catalyst solutions were first prepared in the drybox as described above with [Ir] = 0.6 mM, Al/Ir = 2.0, and an initial cyclohexene concentration of 1.65 M. Each poisoning experiment used ≥ 300 equivalents of Hg(0) per Ir added in the drybox. Thorough contact of the insoluble Hg(0) and the catalyst in solution was ensured by stirring at 1000 rpm

in the sealed FP bottle in the drybox for 24 h. For poisoning after a partially completed hydrogenation run, the hydrogenation reaction was quenched by filling and purging with 40 psig of Ar gas five times (once every five seconds). The FP bottle was then transferred back into the drybox where Hg(0) was added. After the 24 h mixing period, the sealed FP bottle was again removed from the drybox, and hydrogenation was resumed according to the procedure already described. Time and pressure values then collected have been corrected to fit with the initial portion of the data, Figure 12. Control experiments show that 24 h of mixing the catalyst solution with Hg(0) is necessary and sufficient for catalyst poisoning (Figure S35, Supporting Information) and that the experimental procedure itself is not the cause of the loss of catalytic activity. Another control experiment showed that, for poisoning of the initial catalyst, before a hydrogenation run was started, removal of the Hg(0) from the catalyst solution made no difference in the result.

Z-Contrast Microscopy. Samples of the $[(1,5-COD)Ir(\mu-O_2C_8H_{15})]_2$ plus $AlEt_3$ catalyst (3.00 mL, 1.00 mM in [Ir], with an Al/Ir ratio of 2.0) were collected for Z-contrast microscopy both before and after use in cyclohexene hydrogenation, double-sealed airtight, and shipped to the Center for Microanalysis of Materials (CMM), University of Illinois at Urbana–Champaign (UIUC) for imaging. Grid preparation for Z-contrast microscopy was conducted in a glovebag filled with dry N_2 at > 1 atm and located in the TEM room. The solution sample was diluted with cyclohexane to twice its original volume. Next, 2–3 drops were dispersed onto a TEM grid with an ultrathin carbon film on a holey carbon support (Ted Pella, Inc.) and dried at room temperature under N_2 for ≥ 10 min. Once dried, a TEM grid was transferred quickly into the TEM column to reduce oxidation of the sample. Images were acquired using a field-emission JEM 2010 (scanning) transmission electron microscope operated at 200 kV. The samples were first treated with a high-intensity electron beam (electron beam shower) for ~15 min each time in the TEM column (with vacuum better than 3×10^{-6} Torr) to assist in high quality imaging. The high-angle scattering electrons were collected with a JEOL ADF detector at a camera length of 8 cm, with a 0.2 nm (nominal) diameter probe. High-angle annular dark-field (HAADF) images were collected at 2 M (million) magnification and were 1024×1024 pixels in dimension. Cluster diameters were measured at the full width at half-maximum (FWHM) of the intensity profile across ≥ 600 clusters from images at the same levels of magnification and contrast (an example intensity profile is shown in the Supporting Information).

XAFS Spectroscopy. Sample solutions were prepared at CSU in 6.0 mL batches at 5.0, 6.0, or 7.2 mM in [Ir]. Containers were double-sealed airtight and transported to the National Synchrotron Light Source (NSLS) at Brookhaven National Laboratory (BNL), Upton, New York (two days transit time). At the NSLS, all catalyst samples were handled and stored in a N_2 atmosphere glovebox maintained at ≤ 10 ppm O_2. Solution samples were loaded into a custom-designed airtight sample cell composed of a stainless steel frame made to press Kapton film windows onto a Teflon block with a ~1.5 mL sample cavity. The samples were loaded using glass pipettes into threaded ports in the Teflon block, which were then sealed using Teflon screws. Airtight seals in the threaded ports and windows were ensured by using Kalrez o-rings.

A portion of the Al/Ir = 1.0 catalyst sample was used for catalytic hydrogenation of cyclohexene and then collected for XAFS analysis. The brown solution had precipitated as a dark brown powder in transit to the NSLS where the XAFS experiments were performed. This is not unusual however because, as already noted, catalyst solutions kept in the drybox sometimes precipitate within a few days after completion of a catalytic run. The powder was isolated by centrifugation followed by evaporation in vacuuo. The powder was then brushed onto the adhesive side of a strip of Kapton tape. The tape was then folded repeatedly and held in place with additional Kapton tape to

(77) Shriver, D. F.; Drezdzon, M. A. *The Manipulation of Air-Sensitive Compounds*, 2nd ed.; John Wiley and Sons: New York, 1986.

(78) Watzky, M. A.; Finke, R. G. *J. Am. Chem. Soc.* **1997**, *119*, 10382–10400.

(79) Widegren, J. A.; Aiken, J. D., III; Özkar, S.; Finke, R. G. *Chem. Mater.* **2001**, *13*, 312–324.

ensure an airtight seal. Reference samples of Ir black and $Ir_4(CO)_{12}$ powders were prepared in this manner; however, preparation of Ir black was done outside the drybox. As already mentioned, a lack of contamination by atmospheric O_2 during posthydrogenation XAFS analysis was confirmed from the XAFS, XANES, and independently performed XPS results, all showing that the sample consisted of Ir(0). Control experiments were performed to test whether the treatment of catalyst material necessary for analysis by XAFS and XANES *after* use in cyclohexene hydrogenation affects its activity. Samples of the catalyst after their use for cyclohexene hydrogenation were collected by bringing the F−P bottle back into the drybox after the H_2 consumption had ceased and removing the cyclohexane solvent under a vacuum. This provided isolated catalyst powder analogous to that analyzed by XAFS and XANES. The powder was then redissolved in 2.5 mL of cyclohexane and transferred into a new culture tube in an F−P bottle followed by 0.5 mL of cyclohexene. A second cyclohexene hydrogenation performed following this treatment gave the activity results shown in Figure 11.

XAFS experiments were performed on a bending magnet beamline, X18b of the NSLS, which uses a Si(111) channel-cut monochromator. X-ray absorption data were collected at room temperature. Samples were mounted and positioned at 45° in the beam path with the help of a motorized sample stage. Gas ion chamber detectors were used for incident, transmitted, fluorescence, and reference channels. Absorption edge calibration was performed prior to XAFS scans using an Ir black standard, for which energy was swept from 150 eV below to 1800 eV above the Ir L3 edge (11 215 eV). Energy was swept from 150 eV below to 2000 eV above the Ir L3 edge for all other samples, except in the case of data collection on the [(1,5-COD)Ir(μ-$O_2C_8H_{15}$)]$_2$ precatalyst, when the energy was swept to 1800 eV above the L3 edge. Reference spectra were obtained simultaneously in the transmission mode for all sample scans using the Ir black standard. The number of scans performed was 2, 29, 6, and 9 for Ir black, HPO_4-stabilized Ir nanoclusters, $Ir_4(CO)_{12}$, and [(1,5-COD)Ir(μ-$O_2C_8H_{15}$)]$_2$, respectively. For the Al/Ir = 0.5, 1.0, 1.5, 2.0, 2.5, 3.0, and 5.0 catalyst samples before hydrogenation, 5, 5, 10, 10, 10, 3, and 6 scans were performed, respectively. Three scans were performed on an Al/Ir = 10.0 sample, but the data were excessively noisy (Figure S22, Supporting Information), precluding reliable analysis and fitting. For the Al/Ir = 1.0 sample after hydrogenation, 17 scans were performed. Fluorescence data were deemed inferior in quality to the transmission data and therefore disregarded.

Data processing was accomplished using IFEFFIT.[80] The reference spectra were used for scan alignment. The threshold energy (E_0) was assigned a value that corresponded to approximately half the normalized edge step, 11 213 eV, and multiple scans of a single sample were merged (averaged). The range of data deemed to have a sufficient signal-to-noise ratio was selected using a Hanning window function for Fourier transforms (FTs), Figures S10−S21 of the Supporting Information.

A drift in the scans of the Al/Ir = 1.5, 2.0, and 2.5 catalysts before hydrogenation was observed, Figure S24, Supporting Information. A control experiment performed in an attempt to rule out possible sample damage caused by the X-ray beam suggests that no beam damage was occurring, Figure S25, Supporting Information. The reason for the observed drift is not apparent, but to lessen its effect on the analysis, the first two scans in each case were merged, and the others were discarded.

Supporting Information Available: Additional experimental information and control experiments for cyclohexene hydrogenations. Bright-field TEM images, corresponding particle size histograms, and images from TEM and HRTEM control experiments. MALDI mass spectra and results of associated control experiments. XAFS spectra with fits, tables of fitting results, and associated XAFS control experiments. Survey and high-resolution XPS spectra. HR and other TEM images of catalysts after hydrogenation. XAFS-determined coordination number-particle diameter correlation curve. Hg(0) poisoning control experiments. A full list of the authors of reference 6d. This material is available free of charge via the Internet at http://pubs.acs.org.

(80) (a) Newville, M. *J. Synchrotron Radiat.* **2001**, *8*, 322–324. (b) Ravel, B.; Newville, M. *J. Synchrotron Radiat.* **2005**, *12*, 537–541.